Charmonium suppression in heavy-ion collisions

C. Gerschel
Institut de Physique Nucléaire
F - 91406 Orsay Cedex, France

and

J. Hüfner
Institut für Theoretische Physik der Universität Heidelberg
Philosophenweg 19
D - 69120 Heidelberg, Germany

CONTENTS

1 INTRODUCTION

Heavy ion collisions at high energies promise rich physics, but it is not obvious how to uncover it. A situation like this is quite normal, when a new field of physics opens. Data are taken and hypotheses are proposed, but facts and theories do not fit together. The history of charmonium suppression in high-energy heavy ion collisions is a good example. In 1986, Matsui and Satz [1] suggested that the expected transition from hadronic matter to deconfined matter, the quark-gluon plasma (QGP), could be accompanied by a strong J/ψ suppression and indeed a suppression of J/ψ production was observed for the first time in 1989 by the NA38 collaboration [2] in O-U collisions at 200 GeV/c per nucleon and a year later in S-U collisions at the same energy [3]. In the following years, the data from proton-nucleus collisions (pA) and nucleus-nucleus collisions (AB) have become more abundant and precise and revealed in particular two surprises: i) J/ψ and ψ' are equally suppressed in pA collisions and ii) the heavy ion data then available are compatible with predictions based on the results from pA collisions, where a QGP is not expected to be formed. On the theoretical side many effects which contribute to suppression in pA collisions have been analyzed and understood. The year 1996 has brought a new surprise: in Pb-Pb collisions the observed J/ψ suppression is considerably stronger than expected on the basis of previous data from pA and SU collisions. Explanations have been quickly at hand and numerous.
In this situation it may be useful to critically review the state of the field, bring the data together and discuss their interpretations. This will be done in this paper. We have organized the review in the following way: The experimental set-up and all the data from heavy ion collisions are presented in chapter 2. Then the data and the theoretical ideas about charmonium production in pp and suppression in pA collisions are reviewed as far as they are relevant for heavy ion collisions. Finally, in chapter 4, the data for J/ψ and ψ' suppression in O-Cu, O-U, S-U and Pb-Pb collisions are compared with extrapolations based on pA data in order to bring out the new physics. The various explanations are described. The present review is devoted to the suppression in heavy ion collisions and we have attempted to be complete in the presentation of their physics, while the reader should not expect completeness in the wider field of hadronic charmonium production and suppression. We have included publications (even on the web) until the end of 1997. Figures related to NA38 and NA50 experiments are adapted from figures which can be found in the references concerning these two experiments.

2 MEASUREMENTS WITH HEAVY IONS

Charmonium production in heavy ion collisions has been measured at the CERN SPS by the NA38 and NA50 experiments. J/ψ and ψ' resonances

are recognized through their decay channel into a muon pair. In the measurement of dimuons Drell-Yan pairs are also recorded. They will be used as a reference to study J/ψ suppression.
NA38 has been devoted to the study of collisions induced by 200 GeV/nucleon oxygen and sulphur projectiles and also by 200 and 450 GeV/c protons. The NA50 detector is dedicated to experiments with 158 GeV/nucleon Pb projectiles. It is an upgraded version of the NA38 apparatus and is designed to cope with the increased radiation level and the larger multiplicities and background related to Pb projectiles. The NA50 set-up is described in this review. The differences to NA38 are indicated. More details about NA38 and NA50 set-ups can be found in references [2] and [4].

2.1 Experimental set-up

The experimental set-up of NA50 [4] is shown in Figure 1. It is made of a muon spectrometer which uses the same basic components as the spectrometer of the NA38 experiment [2]: a toroidal magnet bends the muon tracks which are measured by 8 multiwire proportional chambers (PC1 to PC8). The muon pair trigger is provided by four hodoscopes of plastic scintillators (R1 to R4). The trigger efficiency is measured from two other hodoscopes (P1 and P2).
Hadrons produced in the collision are filtered in an absorber before they decay into muons in order to reduce the number of background muon pairs as far as possible. This absorber is made of a 60 cm long conical BeO preabsorber, starting 25 cm after the end of the target assembly, followed by a 4 m carbon and 80 cm iron absorber. The absorber is located in the acceptance of the spectrometer (35-140 $mrad$) as indicated in Figure 2. The beam is dumped inside the carbon-iron absorber into a tungsten-uranium beam plug.
Details about the target region are shown in Figure 2. The target itself is an "active" segmented one, "active" because it is designed to recognize the precise vertex of the interaction and a possible reinteraction of a spectator fragment in a subsequent subtarget which would spoil the determination of the centrality of the collision. It is made of 7 Pb subtargets followed each by two quartz blades located off the beam axis.
The centrality of the collision can be estimated from three detectors, an electromagnetic calorimeter, a "zero degree" calorimeter and a multiplicity detector. The electromagnetic calorimeter is made of scintillating fibers embedded in a 14 cm thick Pb-converter. It measures the energy of particules in a pseudo-rapidity range [1.1 - 2.3]. Its resolution is 5% for central Pb-Pb collisions. A contamination due to charged particles amounts to about 40% to the measured transverse energy. It is estimated using a Monte-Carlo simulation and subtracted from the measured spectrum in order to obtain the neutral transverse energy spectrum.
The zero-degree calorimeter measures the energy carried away by the beam

spectators. It is located inside the hadron absorber at the beginning of the beam plug with its front face 165 cm from the target center. It is is 65 cm long and is made of quartz fibers embedded in a tantalum converter. The transverse section of the calorimeter is 5×5 cm^2. In order to minimize the contamination of particles produced in the collision, its angular acceptance is defined by a 60 cm long Cu collimator. The energy resolution is 7% for 32.7 TeV incident Pb-ions.
Finally, a multiplicity detector made of two planes of silicon strip detectors measures charged particles in the rapidity range [1.5 - 3.9]. Its information is not yet available for the results discussed in this review.
In addition, a beam hodoscope is used for three purposes: i) to identify and count the incident ions, ii) to reject events where two or more ions are present in the reading gate of the detectors (duration of 20 ns for most of them) and iii) to precisely time the dimuon trigger with a jitter less than 1 ns. The hodoscope is made of a single plane of 16 quartz counters and is located 22 m upstream from the target in a place where the beam spot is large enough to induce acceptable individual counting rates. It is followed immediately downstream by 6 auxiliary plastic detectors which are located off the detector acceptance and which tag, for off-line rejection, the events where the beam has interacted in the detector itself.
The main differences with respect to NA38 set-up are the following:

- The spectrometer is compressed in order to have the same c.m.s rapidity range $0. < y_{cms} < 1.$ after the change of the beam energy from 200 to 158 $GeV/$nucleon.
- The current in the magnet is increased from 4000 to 7000 A. Together with the removal of the electromagnetic calorimeter from the acceptance of the spectrometer [1] and its replacement by the BeO absorber, the mass resolution is substantially improved: $\sigma_\psi = 96$ MeV instead of 145 MeV. This gain is very important in order to insure a better mass separation between J/ψ and ψ' .
- In NA38, the electromagnetic calorimeter was the only "centrality" detector but it covered a larger pseudo- rapidity domain.
- In the "active" target and the beam hodoscope, strongly exposed to radiation damage, the plastic scintillators previously used in NA38 experiment are replaced by quartz based detectors which are more radiation resistant by a factor about one thousand. This has not been necessary for the electromagnetic calorimeter which is only used in the backward hemisphere of NA50.
- Finally, because of the location of the BeO preabsorber close to the target end, the number of back-ground pairs due to the decay of pions

[1] In NA38, particles were measured in the pseudo-rapidity range [1.7 - 4.1]. Multiple scattering of the muons in the Pb-converter of the calorimeter spoiled the mass-resolution of the spectrometer.

and kaons before their interaction in the absorber is not increased too much when going from S-U collisions (NA38) to Pb-Pb collisions (NA50). In the J/ψ region, it is less than 1.5% of the signal events for S-U collisions and increases up to 15% for Pb-Pb central collisions.

Due to the small cross sections of the processes which are studied, the experiments are run at very high luminosities. The thickness of the target is 17.5% of an interaction length for uranium and for the lead data recorded in 1995 and it increased to 30% for the 1996 Pb-run. The luminosity is between 1 and 3 10^6 interactions/s.

2.2 Analysis

Recorded events are selected according to criteria described in references [2, 3, 4, 5] which, briefly summarized, require two reconstructed tracks with a common origin in the target region, no reinteraction of a spectator fragment and no pile-up. By requiring the recognition of the precise subtarget where the interaction has occured, it is not possible to study very peripheral collisions because the efficiency of the "active" target algorithm is too low for them. Another method has been developped by NA50 [6, 7, 8] which is based on the correlation between the "zero degree" energy and the neutral transverse energy and keeps only events which lie within a 2σ region around the average $E_T - E_{ZDC}$ correlation. The gain in peripheral events is clearly seen when comparing Figures 3 and 4.
Finally, the opposite-sign muon pair sample being contaminated by back ground muon pairs, this background has to be subtracted. It is estimated from like-sign decay muon pairs detected in the spectrometer according to the relation [2] :

$$N_{bg} = 2 \times \sqrt{N^{++} \times N^{--}}, \tag{1}$$

where N_{bg} is the calculated number of $\mu^+\mu^-$ background pairs and N^{++}, N^{--} are the numbers of $\mu^+\mu^+$ and $\mu^-\mu^-$ pairs, respectively. The signal is then defined by $N_{signal} = N^{+-} - N_{bg}$ where N^{+-} is the number of pairs with opposite sign muons.

2.2.1 Acceptances

The analysis is restricted to muon pairs within the kinematical domain where the acceptance of the spectromer is sizable, i.e. with a c.m.s rapidity in the range [0. - 1.] and a polar decay angle of the muons in the Collins-Soper reference frame which satisfies $|cos\theta_{CS}| < 0.5$. The acceptance of

[2] It can be shown that this relation requires that the muon acceptance in the apparatus is the same for μ^+ and μ^-. A fiducial cut is therefore applied which rejects any pair where one muon would have been out of acceptance in the opposite magnetic field.

the Drell-Yan process as a function of mass is shown in Figure 5 for S-U collisions. The acceptances in transverse momentum and in rapidity of J/ψ for the same system are shown in Figure 6.

2.2.2 Mass spectrum analysis

An example of an invariant mass spectrum including background is shown in Figure 7 for Pb-Pb collisions [6]. The spectrum is a superposition of contributions coming from different origins like J/ψ and ψ' resonances, Drell-Yan and background muon pairs. There is also a small contribution from the semi-leptonic decay of D and $\bar{D}$ mesons and possibly from an "excess" whose origin is still not clear [9]. In order to obtain the numbers of J/ψ , ψ' mesons and of Drell-Yan pairs without uncertainties related to this "excess", the invariant mass spectrum is fitted above 3.05 GeV/c^2 where this last component is very small[3]. The fit thus includes four contributions, J/ψ , ψ' , Drell-Yan and background pairs determined from the like-sign pairs as explained above. The number of pairs coming from the $D\bar{D}$+"excess" contribution is obtained from a special fit in the mass region below the J/ψ and then introduced as a fixed quantity in this high mass region. The shape of the J/ψ , ψ' , Drell-Yan and $D\bar{D}$ contributions is determined from Monte-Carlo simulations. Analytical functions are used to smooth the reconstructed simulated events as can be seen in Figure 7. Details about the fit procedure can be found in references [2, 4].

2.2.3 Transverse momentum dependence

The p_T analysis for the different components requires that the experimental spectra are corrected for acceptance and smearing. Two methods have been used and give similar results. The first one [5, 10] is based on an iterative Monte-Carlo procedure where dimuons are generated according to phenomenological laws in each kinematical variable and for each of the components. No correlation between the different variables is taken into account. These "source" functions are propagated through the NA38/NA50 spectrometer, compared to the experimental ones and finally adjusted through an iterative procedure. The second method is based on a 4-dimensional unfolding procedure described in [11]. The main advantage of such a method is that no assumption has to be made neither on the shape of the different kinematical distributions nor on the nature of the particular processes involved in a given mass region. Four dimensional acceptance and smearing matrices are determined using Monte-Carlo programs which simulate the whole apparatus and reconstruction and selection procedures. Details on the method can be found in [11]. Results from both procedure agree well among each other.

[3]For NA38, the lower value of the fit is 2.9 GeV/c^2 because the "excess" is less important.

2.3 Absolute cross sections

Absolute cross sections are computed taking into account the beam intensity measured in the beam detector. Systematic errors of about 7% include all the inefficiencies of identification and reconstruction of the events as well as the effect of the cuts used in order to obtain clean events (such as pile-up cuts for instance). A detailed presentation of all errors can be found in References[4, 14].
For different combinations of target and projectile, J/ψ and ψ' cross sections per nucleon-nucleon collisions in the dimuon channel are shown in Figure 8 [12, 13, 14]. They are compared also to pA collisions. All the cross sections measured at 450 GeV/c are rescaled to 200 GeV/c using a procedure described in reference [4]. The rescaling factor is 0.378 ± 0.034. The *Pb-Pb* cross section is rescaled to 200 GeV/c using the Schuler parametrization [15] which gives a factor 1.32 ± 0.04. The figure also shows a fit to the power law $(AB)^{\alpha}$ which includes all points except *Pb-Pb* for J/ψ and all points except *S-U* and *Pb-Pb* for ψ' . It gives $\alpha_{\psi} = 0.917 \pm 0.011$ and $\alpha_{\psi'} = 0.913 \pm 0.020$. While all J/ψ data agree well from pA to *S-U* collisions, a discontinuity is observed for *Pb-Pb*: the *Pb-Pb* point is much lower than the extrapolation of the fit $(AB)^{\alpha}$.
Also for ψ' a discontinuity is observed. However, it is seen already for *S-U* collisions [4] . It is also observed that for pA collisions, the α-dependence is the same for J/ψ and ψ' . This had been first observed by E772 experiment [16]. For hard processes like J/ψ and ψ' production, one should expect $\alpha = 1$. The deviation from this value is called "J/ψ or ψ' suppression".

2.4 ψ' /ψ ratios

The ratio of ψ' to J/ψ suppression is free from all the uncertainties related to luminosities and flux determination. In Figure 9, the ratio $B'\sigma_{\psi'}/B\sigma_{\psi}$ is plotted as a function of AB for all available data, from NA38 [17], NA50 [8] and other experiments [18]. The solid line corresponds to a fit of the pA data with a power law $k(AB)^{\alpha_{\psi'}-\alpha_{\psi}}$ with $k = 1.75 \pm 0.02\%$, $\alpha_{\psi'} - \alpha_{\psi} = 0.002 \pm 0.007$ and $\chi^2/dof = 0.14$. This results confirms, with a better precision than that of the fits in Figure 8, the observation that J/ψ and ψ' suppressions are the same in pA collisions.

2.5 Centrality of a collision

The "centrality" of an event is defined by the impact parameter b of the collision and cannot be measured directly. It can however be deduced from the measured values of E_T via a model. In both NA38 and NA50 experiments, the centrality of the collisions is determined from the transverse energy spectra of Drell-Yan events with invariant masses above ψ' (Figure

[4]Note that there are no ψ' data for oxygen projectiles due to the lack of statistics in *O-Cu* and *O-U* collisions.

11) [6, 7, 19]. In the figure, the open points correspond to the raw data while the solid points are corrected for the efficiency of the "active" target. It can be seen that this efficiency is very small for peripheral collisions. A simulation of these spectra is made following an improved version of the procedure described in Reference [20] based on a simple geometric model. At a given impact parameter b, the transverse energy is related to the number of "wounded" nucleons [21] of the collision which is calculated using the standard three-parameters Woods-Saxon form with parameters as tabulated in Reference [22]. As in Reference [20], fluctuations in the number of wounded nucleons are introduced. The correlation between E_T and b is thus calculated for each impact parameter and is then convoluted with the probability of having this value of b for a dimuon trigger. The result is shown in Figure 10.

2.6 Centrality dependence of J/ψ and ψ' suppression

The dependence of J/ψ and ψ' suppression as a function of centrality has been studied by using Drell-Yan pairs as a reference. Drell-Yan is a well-known mechanism which produces $\mu^+\mu^-$ pairs of similar features in the same invariant mass range, however with a continuous mass spectrum. In the results presented hereafter, pairs with a mass between 2.9 and 4.5 GeV/c^2 have been used.

The study of the dependence on the centrality of the collision makes use of the neutral energy distribution measured by the electromagnetic calorimeter as shown in Figure 11. The whole samples of muon pairs are divided into different subsamples depending on the transverse energy of the event. In each subsample, a procedure similar to that described in section 2.2.2 is applied and provides the number of J/ψ events and the ratios $B\sigma_\psi/\sigma_{DY}$ and $B'\sigma_{\psi'}/\sigma_{DY}$. B and B' are the branching ratios of the decay of J/ψ and ψ' into two muons. The dependence of the ratio $B\sigma_\psi/\sigma_{DY}$ is shown as a function of the transverse energy of the collision in Figure 12 for *S-U* [19] and *Pb-Pb* collisions [4, 6, 7]. A suppression is indeed observed which increases with E_T, i.e., with the centrality of the collision. This suppression is stronger for *Pb-Pb* than *S-U*: about a factor 3 between the two extreme centrality bins for *Pb-Pb* and only 1.3 for *S-U*.

$B'\sigma_{\psi'}/\sigma_{DY}$ ratios are shown in Figure 5 [8, 19]. Again, one observes a suppression of ψ' which is much stronger than for J/ψ. Between the extreme centrality bins, there is a factor of more than 10 for *Pb-Pb* and about 4 for *S- U*.

2.7 Drell-Yan cross sections

Although thoroughly studied in proton and pion-induced reactions in a wide range of energies [23], Drell-Yan cross sections have not been measured before in nucleus-nucleus collisions. In order to check, if the Drell-Yan me-

chanism remains a good reference, the experimental cross sections have been compared to standard QCD calculations which are known to account for the experimental results in hadron-induced experiments. For AB interactions, the cross section is considered as the sum of elementary pp, pn and nn cross sections according to the numbers of nucleon-nucleon interactions in the colliding nuclei. The calculation is done in leading order using the GRV-LO 1992 set [24] of parton distribution functions. The comparison between the different systems is made through the so-called K-factor which accounts for higher order corrections and which does not depend on the invariant mass of the Drell-Yan pair. K is defined for each system with its specific kinematical domain and $\sqrt{s}$ value, as $K_{DY} = \sigma^{DY}_{exp}/\sigma^{DY}_{GRV-LO}$. The obtained K-factors are shown in Figure 14. They all agree well and suggest that the Drell-Yan mechanism in nucleus-nucleus interactions is still a good reference to study J/ψ suppression.

2.8 Transverse momentum dependence

After corrections for acceptance and smearing as explained in section 2.2.3, p_T-distributions are obtained [8, 25, 26]. Three kinds of informations are available:

- The ratio of the p_T-distribution in a given E_T bin to the same distribution in the first E_T bin is computed after a normalization by the respective values of the Drell-Yan continuum in each bin. It thus gives the evolution of the p_T-dependence of J/ψ suppression with centrality in comparison with the first centrality bin. Such ratios are shown in Figures 15 and 16 for S-U and Pb-Pb collisions. It is observed that for a given centrality bin, the suppression is stronger at low p_T and that it weakens with increasing p_T ($R_{pT} > 1$). This behaviour becomes more pronounced with increasing centrality. It is also stronger for Pb-Pb than for S-U collisions as could be expected from the values of the suppression integrated over p_T. There may be also a saturation effect for $p_T > 3\ GeV/c$ in the Pb-Pb system, but this is not completely clear because of the limited statistics in this p_T region.
- The mean values $< p_T >$ and $< p_T^2 >$ are determined for p_T -distributions integrated over the impact parameter. In Figure 17, the $< p_T^2 >$ values are shown to scale with $A^{1/3}$.
- The mean values $< p_T >$ and $< p_T^2 >$ are also determined as a function of transverse energy [8]. The $< p_T^2 >$ values are shown in Figure 18 for J/ψ . They increase with the centrality of the collision. The increase is stronger for Pb-Pb than for S-U and saturates for more central collisions.
  Figure 19 shows the $< p_T^2 >$ values of ψ' as a function of E_T. The $< p_T^2 >$ values are larger for ψ' than for J/ψ . Because of the lack of statistics, it is difficult to draw any conclusion about the E_T-dependence.

3 CHARMONIUM PRODUCTION IN pp AND AND ITS SUPPRESSION IN pA COLLISIONS

In order to be sure that the J/ψ and ψ' suppressions observed in heavy ion collisions point to new physics, one has to analyze and understand charmonium production in pp collisions and its suppression in pA collisions. In the present chapter we review data and their interpretation as far as they may be relevant for the heavy ion experiments. Thus we restrict ourselves to collisions where the laboratory energy E_p of the incident proton is in the region of hundreds of GeV and where the produced charmonium is observed with $|x_F| < 0.4$.

3.1 J/ψ and ψ' production in pp collisions

The charmonium states of interest in this review are bound states of a charm-anticharm pair $c\bar{c}$ with quantum numbers $n^{2S+1}L_J$, where n is the radial quantum number, and S, L and J denote spin, orbital and total angular momentum, respectively: $J/\psi(1^3S_1)$, $\chi_{cJ}(1^3P_J)$ with $J = 0, 1, 2$ and $\psi'(2^3S_1)$. The states J/ψ and ψ' have the quantum numbers of the photon and can be observed via their decay into $\mu^+\mu^-$. The χ_{cJ} states contribute to J/ψ production via the decay channel $J/\psi\gamma$.

3.1.1 Experimental information

The cross section $d^3\sigma^{pp\to J/\psi X}/dx_F d^2p_T$ depends on the c.m. energy $\sqrt{s}$ of the protons, the fractional momentum x_F in the c.m. system and the transverse momentum p_T of the produced J/ψ. The integrated cross section for $pp \to J/\psi X$ depends rather strongly on energy and the data for $\sqrt{s} < 60\ GeV$ are conveniently parametrized by [15]

$$\sigma^{pp\to J/\psi X}(s, x_F > 0) = \sigma_0 \left(1 - \frac{M_{J/\psi}}{\sqrt{s}}\right)^n \tag{2}$$

with $\sigma_0 = 638 \pm 104\ nb$ and $n = 12.0 \pm 0.9$ (Figure 20). The x_F dependence is symmetric around $x_F = 0$. It drops to one half of the central value at $|x_F| \approx 0.2$. The distribution in transverse momentum p_T (Figure 21) can be characterized by a mean squared momentum [27] $< p_T^2 >= (1.23 \pm 0.05)(GeV/c)^2$.

A sizeable contribution of the observed J/ψ's arises from the decay of the excited charmonium states χ_{c_1}, χ_{c_2} and ψ'. Their contributions are at 300 GeV [28]

$$\begin{aligned} P(\chi_{c_1} + \chi_{c_2} \to J/\psi\gamma) &= (30 \pm 4)\% \\ P(\psi' \to J/\psi 2\pi) &= (7.5 \pm 1.7)\% \end{aligned} \tag{3}$$

relative to the observed J/ψ intensity. The apparent yield of ψ' relative to J/ψ in the $\mu^+\mu^-$ channel is rather small [8]

$$\frac{\sigma^{pp\to\psi' X}\cdot B(\psi'\to\mu^+\mu^-)}{\sigma^{pp\to J/\psi X}\cdot B(J/\psi\to\mu^+\mu^-)} = (1.64\pm 0.03)\% \tag{4}$$

because of the small branching ratio $B(\psi'\to\mu^+\mu^-)$ and makes the study of ψ' suppression difficult. Within the error bars, the ratio Equation (4) depends rather little on energy [29]. If one corrects for the branching ratios B and for the decays $\psi'\to J/\psi$ and $\chi_c\to J/\psi$ one deduces

$$\frac{\sigma_d^{pp\to\psi' X}}{\sigma_d^{pp\to J/\psi X}} = 0.21\pm 0.05 \tag{5}$$

for direct production of the two charmonium states. We note that the same value (within error bars) for the ratio (5) is observed in photoproduction $\gamma p\to J/\psi X$ [30].

3.1.2 Mechanisms for charmonium production

An important scale in charmonium physics is set by the mass m_c of the charmed quark. Its value $m_c\approx 1.5\ GeV$ is considerably larger than $\Lambda_{QCD}\approx 0.2\ GeV$ and this fact permits perturbative expansions in $\alpha_s(m_c)$. Furthermore, potential models describe the charmonium states fairly well [31]. These yield wave functions for the charmonium states, necessary ingredients for calculations of decay, production and suppression. For order-of-magnitude calculations one may consider the charmonia as $1s$, $1p$ and $2s$ states in a non-relativistic harmonic oscillator model with frequency $\omega=(M_{\psi'}-M_{J/\psi})/2=0.3\ GeV$.

Production of charmonium is a complicated theoretical problem mainly because of the non-perturbative aspects of bound state formation. The production of the $c\bar{c}$ pair is usually treated separately from its evolution into a bound state (factorization), since the two processes differ by their scales, m_c and $\Delta M = M_{\psi'}-M_{J/\psi}$, respectively. In the present subsection the three main models for hadro-production of charmonia are described in their historical order. Two recent reviews [15] and [32] are recommended for more details. As an example we give expressions in the various models for J/ψ production in pp collisions via the three-gluon fusion mechanism, which is not the only one, but dominates at high energies.

The color evaporation model has been developed in references [33, 34]. The following expression contains the essential physics:

$$\begin{aligned}\sigma_{CE}(pp\to J/\psi X, x_F; s) &= f_{J/\psi}\int_{4m_c^2}^{4M_D^2} d\mu^2 \int dx_1 dx_2 \delta(x_F-x_1-x_2)\\ &\quad\times g(x_1)g(x_2)G_2(gg\to[c\bar{c}](\mu^2);\hat{s}).\end{aligned} \tag{6}$$

Two gluons with fractional momenta x_1 and x_2 ($\hat{s}=x_1x_2s$) fuse to form a $c\bar{c}$ pair with mass μ but otherwise unspecified quantum numbers. The

elementary cross section G_2 is calculated perturbatively to order α_s^2 and is folded with the gluonic structure functions $g(x)$ in the proton. The colored $c\bar{c}$ pair develops - via an unspecified mechanism called color evaporation - to a bound charmonium state, if the mass μ satisfies $4m_c^2 < \mu^2 < 4M_D^2$, i.e. lies between the $c\bar{c}$ production and the open charm decay thresholds. A phenomenological factor $f_{J/\psi}$ gives the fraction of the intensity which goes to the J/ψ. The model reproduces the $\sqrt{s}$, x_F and p_T dependence of charmonium production in pp collisions, but cannot estimate absolute cross sections. It predicts ratios of production rates of different states to be independent of $\sqrt{s}$, as observed experimentally. A recent comparison with experiment can be found in [35].

The color singlet model developed since 1980 [36, 37, 38] includes the quantum numbers of the produced charmonium states explicitly. It may be characterized by the following expression

$$\sigma_{CS}(pp \to J/\psi X, x_F, p_T; s) = |R_{J/\psi}(0)|^2 \int dx_1 dx_2 \times \int d^2p_T' d^2p_T'' \delta(x_1 + x_2 - x_F) g(x_1, p_T') g(x_2, p_T'') \times G_3(gg \to [c\bar{c}]_{J/\psi} + g; M_{J/\psi}^2, x_F, p_T; \hat{s}, p_T', p_T''). \quad (7)$$

The elementary cross section G_3 describes a $3g$ process which leads to the creation of a $c\bar{c}$ in the color singlet state (therefore the name) with the quantum numbers and the mass of the J/ψ. The radial wave function $R_{J/\psi}(0)$ at the origin determines the probability that this $c\bar{c}$ pair is a J/ψ. The cross section G_3 proportional to α_s^3 in leading order, is to be folded with the x and p_T-distribution of the initial gluons. The "primordial" p_T-distribution carried by the gluons together with the amount of p_T carried away by the third gluon determines the p_T distribution of the J/ψ. For a detailed discussion of cut-off dependences and for a comparison with experiment we refer to the review [15].

The color octet model has been introduced by [39] in a study of the decay $\chi \to q\bar{q}g$. It has received particular interest [40] in connection with the data for J/ψ with $p_T \geq 5\ GeV/c$ produced in $p\bar{p}$ collisions at $\sqrt{s} = 1.8\ TeV$, where dramatic discrepancies with respect to predictions of the color singlet model have been discovered [41]. The basic idea is contained in the following expression (where for clarity we have dropped the p_T and x_F dependences):

$$\sigma_{CO}(pp \to J/\psi; s) = \sum_n \langle O_n^{J/\psi} \rangle \int dx_1 dx_2 g(x_1) g(x_2) \times G_3(gg \to [c\bar{c}]_n + X; \hat{s}), \quad (8)$$

where a $c\bar{c}$ is created with the quantum numbers n (color, angular momentum and spin) and where $\langle O_n^{J/\psi} \rangle$ is proportional to the probability to find the point-like $[c\bar{c}]_n$ in the wave function of the J/ψ. If n refers to the quantum numbers of the J/ψ, one has $\langle O_n^{J/\psi} \rangle = |R_{J/\psi}(0)|^2$ and one recovers the color singlet model. For a colored $[c\bar{c}]_n$, $\langle O_n^{J/\psi} \rangle$ measures the strength

Exp	Ref.	Targets	E_p (GeV)	x_F	α_ψ
NA3	[27]	H,Pt	200	> 0	$0.94 \pm .03$
NA38	[14]	Cu,W,U	200	[0.,0.37]	$0.91 \pm .03$
NA38/51	[14]	H,D,C,Al,Cu,W	450	$[-.19, 0.14]$	$0.922 \pm .016$
E772	[16]	D,C,Ca,Fe,W	800	> 0.15	$0.919 \pm .005$
E789	[42]	Be,C,W	800	[-0.023,0.032]	$0.888 \pm .025$

Table 1: Experimental information on J/ψ suppression in pA collisions. The α value for NA38 includes also O-Cu, O-U and S-U data.

of a $|[c\bar{c}]_n g\rangle$ Fock space component in the wave function of the J/ψ. Ref. [32] reviews this model and its relation to the data. This model has been extended to the description of pA data (cf. Section 3.2.5).

3.2 J/ψ and ψ' suppression in pA collisions

The various data on J/ψ and ψ' production and their suppression in pA collisions are conveniently presented and discussed in terms of the so-called suppression (or survival) function $S^A_{J/\psi}(x_F, p_T; E_p)$ defined by

$$S^A_{J/\psi}(x_F, p_T; E_p) = \frac{1}{A} \frac{d^3\sigma^{pA\to J/\psi X}}{dx_F d^2p_T} \Big/ \frac{d^3\sigma^{pN\to J/\psi X}}{dx_F d^2p_T}, \tag{9}$$

which relates the nuclear cross section to the one on a nucleon.

3.2.1 Empirical systematics

The A-dependence of the nuclear suppression is currently parametrized in the form

$$S^A_{J/\psi}(x_F, p_T; E_p) = A^{\alpha_\psi - 1}, \tag{10}$$

where any dependence on x_F, p_T and E_p is to be found in the parameter α_ψ. Table 3.1 summarizes values for α_ψ extracted for J/ψ from different experiments. Within error bars there is no energy dependence visible. All the values are integrated over p_T. The suppression is rather constant in x_F for $0 < x_F < 0.3$ and then becomes stronger. Note that the deviation $1 - \alpha_\psi \simeq 0.08$ is rather small. (In the limit of strong absorption one expects $\alpha_\psi = 2/3$).

Parametrizations of the suppression function for other hadronic particles can be found in [43]. Here we quote only two results from $\gamma A \to J/\psi X$ experiment. Reference [44] which uses a bremsstrahlung spectrum with end point $E_0 = 20\ GeV$, but records only one muon (so that the J/ψ cannot

be reconstructed), reports $\alpha_\psi = 0.94 \pm .02$. Tagged photons of energies within 80 - 190 GeV are used by [45] and a value $\alpha_\psi = 0.94 \pm 0.02 \pm 0.03$ is extracted.
The present experimental information about the suppression of the ψ' can be easily summarized: J/ψ and ψ' are suppressed in the same way, i.e. $\alpha_{\psi'} = \alpha_\psi$ for the values of A, x_F, E_p so far investigated. This surprising result has first been discovered by the E772 collaboration[16] with 800 GeV/c protons. (Figure 22).
The dependence of J/ψ suppression on the transverse momentum p_T of the observed J/ψ can be well described, when the experimental cross sections are parametrized in a factorized form

$$\frac{d\sigma^{pA\to J/\psi}}{dx_F d^2p_T}(x_F, p_T; E_p) = \frac{d\sigma^{pA\to J/\psi X}}{dx_F} \cdot \phi(p_T^2/\langle p_T^2\rangle)/\langle p_T^2\rangle, \tag{11}$$

where the mean value $\langle p_T^2\rangle(x_F, A; E_p)$ carries the dependence on A, x_F and E_p. An exemple of the p_T-distribution for pPt collisions is displayed in Figure 21. It shows an increased width as compared to pp collisions. The suppression function $S_\psi^A(p_T)$ for fixed x_F is a ratio of two nearly Gaussian distributions with different widths. Since $\langle p_T^2\rangle$ increases with A, one has $S_\psi^A(p_T) < 1$ for small p_T and an enhancement, $S_\psi^A > 1$, for large p_T. Empirically [27] $\langle p_T^2\rangle(x_F, A)$ depends weakly on x_F for $0 < x_F < 0.3$. The dependence on the nucleon number is conveniently parametrized in the form

$$\langle p_T^2\rangle_{J/\psi}^{pA}(A) = \langle p_T^2\rangle_{J/\psi}^{pp} + cA^{1/3}(A-1)/A \tag{12}$$

as shown in Figure 17.

3.2.2 L-scaling

The data on nuclear J/ψ suppression can also be parametrized in the form [46]

$$S_{J/\psi}^A(x_F, p_T; E) = e^{-\sigma_{abs}(J/\psi)\rho_0 L}, \tag{13}$$

where L is the mean length of the trajectory of the produced $c\bar{c}$ pair in nuclear matter and ρ_0 is the nuclear density. For a uniform density one has $L = \frac{3}{4} r_0 A^{1/3}(A-1)/A$ and $\rho_0 = \left[\frac{4\pi}{3} r_0^3\right]^{-1}$. The parameter to be obtained from a fit to the data is $\sigma_{abs}(J/\psi)$. It is an absorption cross section measured in the experiment, where a J/ψ is observed, but it must not necessarily be the absorption cross section of the finally detected J/ψ. We will come back to this question in Section 3.2.5. We define the mean free path by $\lambda = (\sigma_{abs}\rho_0)^{-1}$. The advantage of Equation (13) lies in its intuitive meaning and in the possibility that it can be extended to heavy ion data as L is a geometrical quantity which is related to the impact parameter and therefore (in heavy ion collisions) to the transverse energy E_T. Of course, the two parametrizations, equations (10) and (13), are not independent and for the

uniform density the absorption cross section σ_{abs} is related to $1-\alpha_\psi$ by

$$\sigma_{abs}(J/\psi) = \frac{16\pi}{9} r_0^2 (1-\alpha_\psi) \ln A/A^{1/3}. \tag{14}$$

Although the A-dependence of the two parametrizations is slightly different, which reflects itself in the factor $\ln A/A^{1/3}$ in Equation (14), this factor equals 1 within 10% for $30 \leq A \leq 200$ and experiments are not sufficiently precise to prefer one of the two parametrizations. In the uniform density model the absorption cross section depends on the radius constant r_0. For $r_0 = 1.1\ fm$, $1-\alpha_\psi = 0.08 \pm 0.01$ and $A = 100$, $\sigma_{abs}(J/\psi) = (5.4 \pm 0.7)\ mb$. One then has a value for the mean free path of $\lambda = 10\ fm$.

3.2.3 Charmonium suppression as a classical phenomenon

On the expectation of QGP formation, Matsui and Satz [1] had predicted J/ψ suppression in heavy ion collisions. When the first data of NA38 had come out, alternative explanations were proposed, among them the following classical picture [47, 48, 49] which we describe for a pA collision. The incoming proton creates a J/ψ instantaneously at point b, z inside the nucleus. On its way out, the J/ψ is attenuated by an exponential damping. The suppression factor is calculated as

$$S^A_{J/\psi} = \frac{1}{A} \int d^2b dz \rho(b,z) \exp\left(- \int_z^\infty dz' \sigma_{abs}(J/\psi) \rho(b,z') \right). \tag{15}$$

Strictly speaking there should be a factor $(A-1)/A$ in the exponent, in order to have no final state effects in pp collisions, but it is negligible in most cases. Expression (15) can be integrated to

$$S^A = \frac{1}{\sigma_{abs}} \int d^2b (1 - e^{-\sigma_{abs} T(b)}) \tag{16}$$

where the index J/ψ or ψ' is omitted. Here the thickness function $T(b) = \int dz \rho(b,z)$ represents the nucleon density per unit area. As long as σ_{abs} is sufficiently small, Equation (16) is well approximated by

$$S^A = e^{-\sigma_{abs} \langle T \rangle / 2} \tag{17}$$

with the mean thickness $\langle T \rangle = \int dz d^2b \rho(b,z) T(b)/A$ and one recovers the parametrization Equation (13) with $< T >= 2\rho_0 L$.
How well does Equation (15) describe the physics of charmonium suppression? Its aspect of final state interactions is supported by the empirical result, that suppression in γA and pA collisions is similar. However, the classical interpretation requires that $\sigma_{abs}(J/\psi)$ is identified with the inelastic $J/\psi N$ cross section $\sigma_{in}^{J/\psi N}$, similarly for ψ'. As explained in the next section, the values for σ_{abs} deduced from pA collisions and the values σ_{in} obtained from other sources do not fit well together. One has to conclude: The object which is attenuated on its way out is neither a J/ψ nor a ψ', but a meson "in the making", which is called a "premeson" or a "pre-resonant state". Its properties are discussed in Section 3.2.5.

3.2.4 The total $J/\psi N$ cross section

We compile information on the $J/\psi N$ total cross section at high energies (tens of GeV) derived from sources other than nuclear suppression. The inelastic $J/\psi N$ cross section $\sigma_{in}^{J/\psi N}$ differs from the total cross section σ_{tot} by the elastic one, σ_{el}. One estimates $\sigma_{el}/\sigma_{tot} = 5\%$. In the following we discuss only the total cross section.

There is no direct measurement of $\sigma_{tot}^{J/\psi N}$ for obvious reasons. However, for vector mesons V like $\rho, \phi, J/\psi$, the value of σ_{tot}^{Vp} is related to data from elastic photoproduction $\gamma p \to Vp$ using the hypothesis of the vector dominance model (VDM) [50]: the reaction $\gamma p \to Vp$ proceeds in two steps: (i) The γ converts into a V and (ii) V scatters elastically on the proton. The VDM has been found successful for the ρ meson. Applied to data $\gamma p \to J/\psi p$ one gets $\left[\sigma_{tot}^{J/\psi N}\right]_{\rm VDM} = 1.2$ mb [30]. Recently, the validity of the VDM has been questioned for J/ψ production [51]: The γ does not convert into a J/ψ, but into a $c\bar{c}$ pair with rather small transverse size and the VDM hypothesis has to be modified [51]. Then one gets

$$\sigma_{tot}^{J/\psi N}(s) = (3.5 \pm 0.15(\exp) \pm 0.6(\text{theo})) \left(\frac{s}{s_0}\right)^{0.22} \; mb \tag{18}$$

for $\sqrt{s} > \sqrt{s_0} = 10\ GeV$, where the first error reflects uncertainties in the experimental input and the second accounts for the theoretical uncertainty. The energy dependence is in line with the observed behavior of $\sigma_{tot}^{pp}(s)$, except that the exponent is larger. The analysis of $\gamma p \to \psi' p$ data within the modified VDM yields a ratio [51]

$$\frac{\sigma_{tot}^{\psi' N}}{\sigma_{tot}^{J/\psi N}} \approx 4, \tag{19}$$

where the accuracy is difficult to estimate.

For high energies ($\sqrt{s} \geq 10\ GeV$), hadron-proton total cross sections σ_{tot}^{hp} are basically geometric in nature. This is revealed by empirical regularities as well as QCD calculations. Empirically [52] one finds a linear relation between the total cross section and the mean squared charge radius of the hadron, e.g.

$$\sigma_{tot}^{hp} = a \langle r^2 \rangle_{ch}^{h}, \tag{20}$$

where a value $a = 5.7$ fits the values for $h = p, \pi$ and K at $\sqrt{s} = 16\ GeV$. Unfortunately, there are no data for the J/ψ m.s. charge radii. If one adds to the calculated value $\langle r^2 \rangle_{J/\psi} = 0.044$ [31] an estimated contribution $1/m_c^2$ to account for the form factor of the quarks [52], Equation (20) leads to $\sigma_{tot}^{J/\psi N} = 4\ mb$ in good agreement with Equation (18).

The empirical systematics (20) finds its theoretical foundation in the Low-model [53], where the elastic hp scattering amplitude (and the total cross section via the optical theorem) is described via two-gluon exchange. In the limit $\langle r^2 \rangle_h \ll \langle r^2 \rangle_p$ one derives Equation (20). The underlying physics is

very simple: The exchanged gluons interact with the hadron via the color dipole operator, which in a first approximation is proportional to the $Q\bar{Q}$ separation r. Double gluon exchange leads to the squared radius r^2. Ref. [54] reports a calculation within this model which yields a value $\sigma_{tot}^{J/\psi p} = 5.75\ mb$, where the difference to the value of 4 mb can be traced to the use of a larger radius. While there may be some uncertainty in Equation (20) on the value of a and on the proper radius operator to take, the basic geometrical nature and the dependence on some $\langle r^2 \rangle$ seem well founded. In particular one expects

$$\frac{\sigma_{tot}^{\psi' N}}{\sigma_{tot}^{J/\psi N}} = \frac{\langle r^2 \rangle_{\psi'}}{\langle r^2 \rangle_{J/\psi}} = 3 \pm 1 \tag{21}$$

depending on the precise values of the radii. This prediction agrees with the empirical result from photoproduction. We draw the attention to references [55, 56] which discuss $J/\psi N$ cross sections also at lower energies.

3.2.5 Space-time structure of charmonium production

We summarize the information for absorption cross sections σ_{abs} derived from the suppression in pA collisions and for total cross sections σ_{tot} obtained from γp data:

$$\begin{aligned} \sigma_{abs}(J/\psi) &= (5.4 \pm .7)\ mb & \sigma_{abs}(\psi')/\sigma_{abs}(J/\psi) &= 1 \\ \sigma_{tot}^{J/\psi N} &= (3.5 \pm .8)\ mb & \sigma_{tot}^{\psi' N}/\sigma_{tot}^{J/\psi N} &\approx 4. \end{aligned} \tag{22}$$

The value 1 of the ratio $\sigma_{abs}(\psi')/\sigma_{abs}(J/\psi)$ as well as the differences between the values σ_{abs} and σ_{tot} both for J/ψ and ψ' are attributed to the finite formation time of the charmonium meson: In a pA collision, the absorption cross sections is that of a premeson, while σ_{tot} relates to a fully developed charmonium meson. In this section we discuss various mechanisms for the space-time structure of the formation process and give values for the formation time τ_f in the c.m.s. of the charmonium and the m.s. value for the transverse separation $\langle r_T^2 \rangle$ which determines the absorption cross sections of the premeson.

In the production of the $J/\psi(\psi')$ via gluon fusion there are three gluons. The approaches differ in their assumptions about the third gluon. If one describes the $J/\psi(\psi')$ formation as a three-step process $gg \to [c\bar{c}]_8 \to [c\bar{c}]_1 + g \to J/\psi + g$, the time scale of the first step is given by $1/2m_c$, and is fast, while the time τ_g for the radiation of the third gluon can be estimated from the uncertainty principle applied to the masses of the octet and singlet+gluon states to be $\tau_g \approx 1/k_\perp$ and depends on the transverse momentum of the gluon. We discuss two alternatives.

- If τ_g is sufficiently small, $\gamma\tau_g \ll R$, one has a color neutral premeson. In an approach based on classical physics [57, 58, 59] the premeson is assumed to be fairly small and to expand to the J/ψ size $\langle r_T^2 \rangle_{J/\psi}$ with

the typical values of the velocity $\langle v_T^2 \rangle_{J/\psi}$ in the J/ψ wave function. In this approach one has

$$\tau_f = \left(\frac{\langle v_T^2 \rangle_{J/\psi}}{\langle r_T^2 \rangle_{J/\psi}} \right)^{1/2} = 0.7 \ fm/c. \tag{23}$$

Since high energy cross sections are proportional to $\langle r_T^2 \rangle$, the absorption cross section is assumed to grow like $(\tau/\tau_f)^2$ for $\tau < \tau_f$.
In a quantum mechanical approach [60, 61] the color singlet wave function $|\phi(\tau)\rangle$ is expanded into a complete set of charmonium states

$$|\phi(\tau)\rangle = |J/\psi\rangle + Re^{-i(M_{\psi'} - M_{J/\psi})\tau} |\psi'\rangle + \ldots. \tag{24}$$

For the transverse separation one calculates at $\tau = 0$ $\langle r_T^2 \rangle = 0.8 \langle r_T^2 \rangle_{J/\psi}$. Since it takes a time τ_f to distinguish energetically between the two states J/ψ and ψ', the formation time τ_f is given by the uncertainty principle

$$\tau_f \approx (M_{\psi'} - M_{J/\psi})^{-1} = 0.3 \ fm/c. \tag{25}$$

- If the third radiated gluon is assumed to be soft one has a colored premeson in nuclear matter [62, 63, 64]. An interesting variant has been proposed by [65]: Starting from the underlying ideas of the color octet model for charmonium production (Section 3.1.2) these authors postulate that the $c\bar{c}$ color octet is dressed by an additional gluon, the whole state $|\,[[c\bar{c}]_8 g]_1\rangle$ being color neutral. This premeson is then a higher Fock state of the J/ψ or ψ' wave function and travels through nuclear matter. The gluon is radiated or absorbed outside nuclear matter. The absorption cross section of the $|\,[[c\bar{c}]_8 g]_1\rangle$ is estimated from the color dipole moment of the $g - [c\bar{c}]_8$ system to be $\sigma_{abs} \approx 9\sigma_{tot}^{J/\psi N}/4$.

Again we draw the attention to the striking similarities for charmonium production in pp and γp reactions and for absorption in pA and γA experiments [66]. Similar physics may underlie the two processes and any theory has to account for it.
Although the various approaches to the structure of the premeson differ considerably, there seems consensus that the transverse size of the premeson is of the order of that for the J/ψ. This explains why the measured value σ_{abs} is not far from σ_{tot} for the J/ψ, but that large differences are to be expected for the ψ'. Since various values for the formation time τ_f are given, it would be very interesting to measure τ_f. This can be done by reducing the energy of the produced $c\bar{c}$, e.g. by detecting the charmonia at smaller, or even better at negative values of x_F. Such negative values can be reached experimentally in inverse kinematics reactions such as Pb projectile on a light target [67]. This will help to understand the real nature of the premeson. Eventually, absorption cross sections and total cross sections should coincide. Also the space-time structure of the χ-states, which can be formed by two gluons, has to be clarified, since they contribute 30% to the J/ψ.

3.2.6 Transverse momentum dependence

While charmonium suppression is basically an effect of the final state, the p_T broadening is attributed to the initial state [68, 69, 70]. A gluon (or quark) of the incoming projectile rescatters from the nucleons inside the target nucleus, before it fuses into a $c\bar{c}$ pair. If one treats the rescattering as a random walk problem one arrives at an expression

$$\langle p_T^2 \rangle_{J/\psi}^{pA} = \langle p_T^2 \rangle_{J/\psi}^{pp} + \sigma_{gN} \langle p_T^2 \rangle_{gN} \rho_0 L_i, \tag{26}$$

where σ_{gN} is the gN elastic cross section, $\langle p_T^2 \rangle_{gN}$ the mean value of p_T^2 in this collision and L_i the mean trajectory length in the target before $c\bar{c}$ formation. For small absorption cross sections of the $c\bar{c}$ pair, the mean trajectory lengths in the initial state L_i and final state L_f are similar. We take $L_i = L_f = L$. The measured slope in Figure 17 can be used to obtain the value for the parameter

$$\sigma_{gN} \langle p_T^2 \rangle_{gN} = (4.5 \pm .4)\ mb\ (GeV/c)^2. \tag{27}$$

We mention that a nuclear dependence of $\langle p_T^2 \rangle$ has also been observed in $\pi A \to l_+ l_-$ Drell-Yan pairs [71, 72]. The difference to the charmonium case is twofold: (i) Drell-Yan pairs have no strong interactions and therefore the observed effect must arise from the initial state. (ii) Drell-Yan pairs arise from $q\bar{q}$ and not gg fusion. Indeed the experiments [71, 72] find a broadening of the p_T-distribution with A which is about a factor of two smaller compared with that from J/ψ production. References [68] and [69] interpret this result in terms of a color factor 4/9 between quarks and gluons.

4 IN SEARCH FOR NEW PHYSICS WITH HEAVY ION COLLISIONS

Do the data for charmonium suppression in experiments with heavy ions point to new physics? This question can only be answered after "new" is defined, i.e., one requires a reference of well-established "old" physics, whose predictions fail for the heavy ion data.

4.1 A benchmark for new physics

The expected new physics in heavy ion collisions is related to the possible creation of extended areas of high energy density, which are not formed in pA collisions. Therefore results from AB collisions should be compared with those from pA collisions. For data with fixed x_F but integrated over p_T and impact parameter, one predicts for J/ψ suppression in AB collisions

$$S_{J/\psi}^{AB}(x_F; AE_p) = S_{J/\psi}^{Ap}(x_F; AE_p) \cdot S_{J/\psi}^{pB}(x_F; E_p), \tag{28}$$

if the suppression in AB collisions is just a superposition of proton-nucleus results. The product on the r.h.s. of Equation (28) needs some discussion.

While good data are available for pB collisions (the second factor) no data exist for the first factor, which is the J/ψ suppression in an experiment with "inverse" kinematics (Ap instead of pA). By changing the reference system one has

$$S^{Ap}_{J/\psi}(x_F; AE_p) = S^{pA}_{J/\psi}(-x_F; E_p). \tag{29}$$

At present pA results are only available for values $x_F > 0$ and an extrapolation to negative values of x_F is not straightforward in view of the formation time effects discussed in Section 3.2.5. For instance at $E_p = 200\ GeV$ the Lorentz factor $\gamma(x_F)$ of the produced $c\bar{c}$ pair drops from $\gamma(0.15) = 16$ to $\gamma(-0.15) = 6$ and this may change the nature of the object which travels in nuclear matter. Since more complete information is lacking, the data for AB collisions have to be compared to the results of pA and pB at the same values of x_F. For instance, the suppression in a $AB \to J/\psi X$ collision measured at a given value of E_T is compared with the reference value

$$\left[S^{AB}_{J/\psi}(x_F, E_T; E_p)\right]_{ref} = e^{-\sigma_{abs}(J/\psi)\rho_0(L_A+L_B)}, \tag{30}$$

where the lengths L_A and L_B for the trajectories of the $c\bar{c}$ in the projectile and target, respectively, are calculated from geometry using the relations between E_T and the impact parameter b, and where $\sigma_{abs}(J/\psi)$ is obtained from the fit to various pA data. In the same way the data for $\langle p_T^2 \rangle$ should be compared with the systematics of Equation (26) where L_i is to be replaced by $L_A + L_B$. The initial state effects may be less influenced by the inverse kinematics.

4.2 Systematics in the length L

4.2.1 Absolute cross sections integrated over E_T

The geometrical length $L = L_A + L_B$, where L_A and L_B are the mean lengths of the $c\bar{c}$ trajectories in the projectile and target nuclei, respectively, is related to the impact parameter b and can be determined from the transverse energy spectrum. The correlation between L and E_T is shown in Figure 23. The cross sections per nucleon-nucleon collisions for J/ψ and ψ' production plotted as a function of L are shown in Figure 24 [5]. We draw the attention to a difference as compared to Figure 8: The cross sections are rescaled to 158 GeV/c for the following reason: If indeed, the Pb points do not follow the systematics of the other data, as we have seen in Figure 8, then we do not know if Schuler's parametrization [15] is still valid for *Pb-Pb* interactions. It is thus more reasonable to rescale the other data to 158 GeV/c. All cross sections of Figure 24 are then divided by 1.32 ± 0.04. Even then the *Pb-Pb* point for J/ψ presents a marked deviation as compared to

[5] Note that the L-values used in this review are calculated with $r_0 = 1.1\ fm$ and with a Woods-Saxon shape for the nuclear density. In previous papers of NA38 and NA50, they were calculated with $r_0 = 1.2\ fm$ and with a uniform density.

the law $exp(-\rho_0\sigma_{abs}(J/\psi)L)$.
For the ψ' , the deviation from the law $exp(-\rho_0\sigma_{abs}(\psi')L)$, valid for pA collisions, appears also for the S-U data. No additional effect is visible for Pb-Pb. The values of the absorption cross sections are $\sigma_{abs}(\psi) = 5.7\pm1.4\ mb$ and $\sigma_{abs}(\psi') = 6.2 \pm 1.5\ mb$.
As explained in section 3.2.3, the exponential law with the parameter L is valid only when σ_{abs} is sufficiently small. A more accurate calculation [73] gives a value of $7.3 \pm 0.6\ mb$ for the absorption cross section of J/ψ .

4.2.2 Centrality dependence

In this section, the values of E_T have been converted into L according to Figure 23. In Figures 25 and 26, the ratios of J/ψ and ψ' cross sections in the dimuon channel to Drell-Yan cross sections are plotted as a function of L. All the cross sections have been rescaled to 158 GeV/c. Moreover, the Drell-Yan cross sections are corrected for isospin effects, i.e. all the nuclei are treated as if they are made of protons only. The Drell-Yan cross section is thus replaced by a corrected value defined by:

$$\sigma_{DY}^{corr} = \sigma_{DY}^{meas} \times \frac{AB \times (\sigma_{DY}^{sim\ LO})_{pp}}{(\sigma_{DY}^{sim\ LO})_{AB}} \tag{31}$$

where $\sigma_{DY}^{sim\ LO}$ are the leading order simulated cross sections for pp and AB collisions. In the first presentations of the J/ψ suppression in Pb-Pb interactions as a function of L from the NA50 experiment [12], Drell-Yan cross sections had been corrected using the GRV LO 1992 [24] set of parton distributions. In more recent papers [6, 7], the MRS 43 [74] set is used since it accounts for the isospin symmetry breaking in the light quark sea of the nucleon as measured by the NA51 experiment [75]. This is important mainly for the 450 GeV/c pp and pd cross sections which are a side-product of NA51 experiment. Figure 24 [8] shows an interesting aspect of the new physics: while for peripheral Pb-Pb collisions (small values of L), the observed suppression follows well the extrapolation of pA and S-U results, the observed suppression suddenly becomes larger with increasing centrality. The discontinuity appears at $L = 8$ fm. One may wonder if above 8 fm, L is still the adequate variable to describe J/ψ suppression? The "anomalous" suppression of J/ψ is quantified in Figure 27 where the experimental values of J/ψ suppression are divided by the absorption values for each E_T bin expected on the basis of the extrapolation of the exponential line in Figure 24. The factor thus defined is compatible with 1 for peripheral collisions. It decreases down to 0.63 ± 0.04 for the more central collisions and is 0.73 ± 0.02 for the integrated cross section: a more than 10 standard deviations from the absorption value!
Note that in the first results of Reference [12], due to the lack of statistics for peripheral collisions, the discontinuity appeared only between S-U and Pb-Pb collisions (Figure 12). This triggered the interpretation of

J/ψ suppression in terms of hadronic comovers effect as explained below. The results shown in Figure 24 are still preliminary. The confirmation of the discontinuity of J/ψ suppression in the $Pb-Pb$ system is of thus of major importance.
For ψ' , no discontinuity is observed in *Pb-Pb* data around 8 fm. The dependences of ψ' production in *S-U* and *Pb-Pb* collisions are rather similar as a function of L. In absolute values, the suppression is even smaller in *Pb-Pb* than in *S-U*, by a factor about 1.5.

4.3 Color deconfinement

The results for J/ψ suppression in *Pb-Pb* collisions cannot be explained by nuclear absorption alone. Other mechanisms have to be considered, the most exciting being the formation of a QGP. We explain the basic idea and its relation to J/ψ suppression.
Hadronic matter undergoes a transition to a deconfined (plasma) phase of quarks and gluons at a temperature T_c between 150 and 200 MeV. In the deconfined phase the properties of charmonium bound states differ significantly from those in the vacuum [1, 76]. The static potential between the c and $\bar{c}$ quarks in the vacuum

$$V(r) = -\frac{4}{3}\frac{\alpha_s(r)}{r} + \sigma r \tag{32}$$

consists of a one-gluon exchange and a confining potential. At finite temperature this potential is screened (cf. Debye screening in an electronic plasma) to

$$V(r,T) = -\frac{4}{3}\frac{\alpha_s(r)}{r}e^{-\mu r} + \sigma r\left(\frac{1-e^{-\mu r}}{\mu r}\right), \tag{33}$$

where $1/\mu(T)$ is called the Debye screening length. To lowest order in the coupling constant g one has $\mu(T) = 1.15gT$ for a plasma with three colors and two massless flavors. According to lattice calculations [77] the perturbative result is a factor of three too low at $T \simeq T_c$. Also the shape of the potential as function of temperature may be more complicated than $V(r,T)$ above [78].
While Reference [76] has investigated the mass shift of charmonium, a quantity difficult to observe, Matsui and Satz [1] have studied the dissociation or Mott temperature T_d, at which a particular charmonium state "melts", i.e. becomes unbound, which phenomenon is observable as additional charmonium suppression. The value of T_d depends on the particular charmonium state, i.e. $T_d = T_c$ is predicted for the dissociation of the ψ' and the χ states, while $T_d = 1.2T_c$ for the J/ψ [79]. In Reference [1], it has been proposed to measure the melting by comparing the production cross sections for J/ψ and Drell-Yan pairs, the latter ones should not feel the QGP. Historically this proposal had triggered the series of experiments reported

on in this review. While the arguments are certainly qualitatively correct, the experience from the electronic plasma suggests that the phenomenon in the QGP may be more complicated [80]. First lattice calculations of the charmonium bound states at finite temperature are available [81]. Irrespective of the fine details, a charmonium state is destroyed, provided it stays in a plasma of sufficiently high temperature and for a sufficiently long time. The minimal time is estimated to be 0.9, 1.5 and 2.0 fm/c for the J/ψ, the ψ' and the χ states, respectively [82].
In a QGP, charmonia may also be destroyed by gluon dissociation [83], i.e. via the reaction $g + J/\psi \to c\bar{c}$, which is the strong interaction analogue of photo-dissociation [84]. Since on the average, massless gluons carry an energy of $3T$ in a plasma of temperature T, their thermal energy is close to or above the charmonium thresholds, if $T \geq T_c$. The relevant dissociation cross section is estimated to a few mb above the threshold for the J/ψ [83]. The relative importance of color deconfinement and gluon dissociation for charmonium suppression in a plasma is discussed in [85].
In the light of the deconfinement effects in a QGP the observed J/ψ suppression in Pb-Pb collisions is interpreted in the following way [86]: Since the J/ψ suppression in S-U collisions follows the pA systematics, there is no indication for a QGP in this reaction. While in peripheral Pb-Pb collisions (relating to small trajectory lengths) the system behaves normal, the observed sudden step at $L = 8\ fm$ is a sign for plasma formation: the ψ' and χ states melt and their contribution to the observed J/ψ yield is strongly reduced. The observed step size of about 35% in the suppression function is in line with this interpretation, since the ψ' and χ states contribute about 40% to the J/ψ yield. A second step in the suppression function possibly present at $L = 9.5\ fm$ is interpreted as the onset of J/ψ melting. This intuitive picture accounts nicely for the structure in the J/ψ data, but it is astonishing that the melting point of ψ' and χ is not seen at all in the ψ' suppression data.

4.4 General threshold model

The step-like structure in the Pb-Pb suppression function invites ideas about threshold phenomena, like the deconfinement transition discussed above. A more general formulation, which includes a threshold, without specifying a particular mechanism has been proposed in [87]. These authors give the following suppression function

$$S^{AB}_{J/\psi}(b) = \int d^2s S^{\rm nucl}_{J/\psi}(b,s)\ \Theta\left(n_{\rm cr} - n_p^{AB}(b,s)\right), \tag{34}$$

where $S^{\rm nucl}_{J/\psi}$ is the suppression expected on the basis of collisions with nucleons alone. It depends on the impact parameter b and s denotes points in the transverse area of the overlap between the two ions. A threshold is introduced by the theta function, which contains the calculated density of participants n_p^{AB} projected on the impact parameter plane. This number is

proportional to the produced energy density [88]. Whenever n_p^{AB} exceeds a critical value n_{cr}, $\Theta = 0$ and the suppression is maximal. The free parameter is the critical density. In Reference [87] it is chosen to be the maximal value of n_p^{AB} ever reached in *S-U* collisions (Figure 28). By construction the suppression in *S-U* collisions is unaffected by this term, but additional suppression of the order of 30% is calculated for the integrated cross section in *Pb-Pb* collisions which agrees with the R_K factor of Section 4.2. Reference [86] extends this model by setting an additional condition: The area where the energy density exceeds a critical value, should be above a certain minimal value - corresponding to the idea that a phase transition needs a certain volume.

4.5 Hadronic comovers

In a hadronic collision (*pp*, *pA* or *AB*) hadrons which are produced together with the $c\bar{c}$ pair are called "comovers". Their asymptotic rapidity distribution dN/dy is well studied. While still in the primordial fireball some of the produced hadrons h may cross the trajectory of the $c\bar{c}$ pair and may destroy the charmonium via an inelastic reaction of the kind $J/\psi + h \to D\bar{D}$ and thus lead to additional suppression. This effect has already been proposed and studied in the year 1988 [89, 90, 91] after the presentation of the first heavy ion data. The suppression due to comovers is usually calculated from an expression of the form

$$S_{J/\psi}^{co} = \exp\left\{-\int d\tau \langle v\sigma_{co}(J/\psi)\rangle \rho_{co}(\tau)\right\}, \tag{35}$$

where $\rho_{co}(\tau)$ is the density of comovers at the location and eigentime τ of the J/ψ. The product $v\sigma_{co}$ (relative velocity and inelastic cross section) is averaged over the kind of comoving hadrons (π, ρ, ...) and their relative energy. The time dependence of the density $\rho_{co}(\tau)$ is taken from an expansion model (often $1/\tau$) with the constraint that the rapidity distribution dN/dy of the observed particles is reproduced. The cross section $\sigma_{co}(J/\psi)$ is an adjustable parameter.

A careful study of comover and other effects on J/ψ suppression for the early results in *O-U* and *S-U* collisions can be found in [92]. Using parameters $v = 0.6$ and $\sigma_{co} = 2\ mb$ these authors find that comovers play a negligible role in *pA* collisions, but contribute significantly to J/ψ suppression in *O-U* and *S-U* reactions especially at large values of E_T. After the discovery of *L*-scaling for *pA* and *AB* collisions the interest in comover effect had decreased since it would destroy the scaling.

The comover discussion is recently revived in an attempt to explain the discontinuity between *S-U* and *Pb-Pb* J/ψ suppressions presented for the first time at QM96 [73, 93, 94, 95, 96, 97, 98, 99]. The cascade calculation [95, 96] provides some interesting insights:

(i) The composition of the comoving hadrons is: $\pi(37\%)$, $\rho(42\%)$, $\omega(13\%)$

and $\eta(8\%)$ (for central *Pb-Pb*). The large fraction of ρ and ω is important, since their reaction with J/ψ into $D\bar{D}$ is exothermic and the corresponding cross section diverges at threshold.
(ii) The relative kinetic energy between the charmonium and its comoving hadron is on the average 0.3 GeV. Therefore high energy results for the $h - J/\psi$ and $h - \psi'$ cross sections do not apply and input from low energy calculations like [56, 100] are needed in order to be sure that the fitted parameters represent the correct physics.
All calculations using comovers reproduce the J/ψ suppression from pA to central *S-U* collisions more or less well. In the calculations $\sigma_{abs}(J/\psi)$ is taken to be between 4 and 7 mb and $\sigma_{co}(J/\psi)$ is adjusted. The fitted values range between 0.4 to 3 mb depending on the assumptions on the density. According to Equation (35) only the product enters. Since the density of comovers does not display a discontinuity as a function of centrality (Figure 28), all calculations based on comover physics cannot reproduce the step in the *Pb-Pb* data of 1997.
The ψ' suppression which deviates from the pA benchmark for *S-U* and *Pb-Pb* collisions is attributed entirely to comovers except in Reference [61] where part of the deviation is explained by formation time effects. While $\sigma_{abs}(\psi')$ for ψ'-N collisions is set to a value between 5 and 7 mb, the $\sigma_{co}(\psi')$ is adjusted to fit the data. The fitted values from the various authors differ significantly, namely between 5 and 25 mb. Nevertheless the observed ψ' suppression is not reproduced very precisely. In this connection an interesting process of enhanced $\psi' \leftrightarrow \psi$ conversion is proposed [101].
Refs. [102, 103] attribute the enhanced observed charmonium suppression in heavy ion collisions to gluon depletion and energy degradation. It is not clear yet how these explanations would also affect the Drell-Yan intensities.

4.6 Transverse momentum dependence

4.6.1 Initial state interactions

The effect of initial state interactions is extrapolated to AB collisions by using $L = L_A + L_B$ in Equation (26). The values of $< p_T^2 >$ for all available data without selection on E_T, are plotted in Figure 29 as a function of L [8]. The results include NA3 data also measured at 200 GeV/c [27]. As explained previously, the data are fitted using the law

$$< p_T^2 >=< p_T^2 >_{pp} + \rho_0 \sigma_{gn} < p_T^2 >_{gn} L. \tag{36}$$

The values obtained are:
$< p_T^2 >_{pp}= 1.21 \pm 0.04\ (GeV/c)^2$
$\rho_0 \sigma_{gn} < p_T^2 >_{gn}= 0.080 \pm 0.007\ fm^{-1}(GeV/c)^2$
with $\chi^2/d.o.f. = 1.4$. A similar figure can be plotted for the centrality dependence of *S-U* and *Pb-Pb* collisions (Figure 30). The *Pb-Pb* results do not show any anomaly around 8 fm where the J/ψ suppression drops

suddenly. They are systematically lower than the S-U data. This may be simply due to the change in the beam energy, from 200 to 158 GeV/c. In the Figure, the dotted line corresponds to plot of the L-dependence using the parameters deduced above from the fit of Figure 29 at 200 GeV/c. It reproduces reasonably well the centrality dependence of S-U collisions. As far as Pb-Pb results are concerned, another fit is made using the above law. It gives, for the parameters at 158 GeV/c:

$< p_T^2 >_{pp} = 1.12 \pm 0.04\ (GeV/c)^2$

$\rho_0 \sigma_{gn} < p_T^2 >_{gn} = 0.077 \pm 0.005\ fm^{-1} (GeV/c)^2$

with $\chi^2/d.o.f. = 1.0$. It corresponds to the solid line in the figure. Most of the beam energy dependence seems to be in the $< p_T^2 >_{pp}$ parameter. A similar dependence of $< p_T^2 >_{\pi p}$ has been observed in the NA3 experiment [27] with incident pions at three different beam energies, namely 150, 200 and 280 GeV.

4.6.2 Other explanations

When the first results on J/ψ production in $O-U$ collisions had appeared the effect of a QGP on the transverse momentum dependence of J/ψ has been studied: References [1, 47, 79] have argued that only $c\bar{c}$ pairs with low p_T will rest sufficiently long inside the QGP and melt without binding, while high p_T J/ψ escape. On the basis of this argument an enhancement in the p_T values is expected in the impact parameter region of QGP formation. There should exist a critical transverse momentum above which J/ψ should no longer be suppressed. That means that the ratios in the figures 15 and 16 should approach 1 at high p_T. It does not seem to be the case at least for S-U, although the statistics in the high p_T region is poor. The situation is less clear for Pb-Pb. It must be noted that this effect should be superimposed on the effect of initial state interactions.

More recently, it has also been argued that the formation of a QGP should lead to a saturation [87, 97] or even to a decrease [104] of $< p_T^2 >$ with L. This is not seen in the data. No new effect seems to be present in the p_T dependence of J/ψ in Pb-Pb collisions.

5 WHERE DO WE STAND?

Coming to the end of this review, it is clear that a tremendous amount of information has been gathered about charmonium formation and suppression in heavy ion collisions both experimentally and theoretically. The most striking features of the data are:

- There is no discontinuity in J/ψ suppression between pp, pA and central S-U collisions. The suppression is governed by the trajectory length L of the J/ψ (or of the premeson) in nuclear matter (L-scaling). The absorption cross section on a nucleon is of the order of 6 mb.

- L-scaling breaks down in Pb-Pb collisions for the most central collisions, above a threshold which is around $L = 8\ fm$.
- The ratio $B'\sigma_{\psi'}/B\sigma_{\psi}$ is constant in pA collisions. This is not the case for heavy ion collisions.
- The suppression of ψ' increases with increasing values of L for heavy ion collisions, but contrary to J/ψ , there is no threshold effect between S-U and Pb-Pb collisions.
- There is also a L-scaling for the p_T-dependence of J/ψ with a universal slope from pp to pA to Pb-Pb central collisions and without any threshold effect.

The interpretation of these empirical laws is not yet satisfactory. For the moment, there is no universal explanation. However, a consensus is reached for some of the above points:

- Charmonium suppression is predominantly an effect of interactions with nucleons in the final state except for central Pb-Pb collisions.
- J/ψ suppression in O-U and S-U collisions shows a continuous evolution from pA collisions. There is thus no need for deconfined matter to explain the data.
- New physics seems to show up in Pb-Pb collisions although its interpretation is not yet clear. However, if the observation of a threshold behaviour inside the Pb-Pb system itself is confirmed, this rules out the interpretation of J/ψ suppression in terms of destructive interactions with comovers.
- The constancy of the $B'\sigma_{\psi'}/B\sigma_{\psi}$ ratio in pA collisions is the result of "premeson" physics: the object which crosses nuclear matter is not yet a J/ψ nor a ψ' . The exact nature of the premeson is still debated.
- The evolution of the $< p_T^2 >$ values of J/ψ from pp to central SU collisions is explained in terms of initial state interactions. This holds also for Pb-Pb collisions where no additional effect is observed.

The nature of the new physics seen in Pb-Pb depends crucially on the existence of one (or even two) thresholds in J/ψ suppression. If the observation is confirmed, it may be a strong support for the formation of deconfined matter in central Pb-Pb collisions and would be a spectacular result in the physics of ultra-relativistic heavy ion collisions. The existence of the threshold should thus be thoroughly studied in the future, e.g. by decreasing the beam energy in Pb-Pb collisions and seeing whether the threshold is shifted towards more central collisions. Then one could conclude that the energy density is the adequate variable to understand the involved physics, as it should be if one deals with a phase transition.
Which kind of new surprises will bring the coming years? We have been used to some spectacular ups and downs which could be revived by the arrival of the new machines such as RHIC and LHC. The story of charmonium suppression in heavy ion collisions has interesting chapters to come.
Acknowledgements: We are grateful to D. Blaschke, D. Kharzeev, and B. Kopeliovich for discussions and advice. We thank B. Chaurand, M. Gonin

for providing some of the figures and Y.B. He and M. Steiert for their help in the preparation of the manuscript. The partial support by the German Ministry for Education and Research (BMBF) via contract 06 HD 856 is gratefully acknowledged.

Literature Cited

1. Matsui T, Satz H. *Phys. Lett. B* 178: 416 (1986)
2. Baglin C, et al. (NA38 Collaboration). *Phys. Lett. B* 220: 471 (1989)
3. Baglin C, et al. (NA38 Collaboration). *Phys. Lett. B* 255: 459 (1991)
4. Abreu MC, et al. (NA50 Collaboration). *Phys. Lett. B* 410: 327 (1997)
5. Baglin C, et al. (NA38 Collaboration). *Phys. Lett. B* 251: 465 (1990)
6. Gonin M, et al. (NA50 Collaboration). RHIC'97 Summer Study, Brookhaven, USA (July 1997)
7. Ohlsson-Malek F, et al. (NA50 Collaboration). International Conference on High Energy Physics, Jerusalem, Israel (August 19-26, 1997)
8. Ramello L,et al. (NA50 Collaboration). Quark Matter 97 Conference, Tsukuba, Japan (December 1-5, 1997)
9. Scomparin E, et al. (NA50 Collaboration). *Nucl. Phys. A* 610: 331c (1996)
10. Baglin C, et al. (NA38 Collaboration). *Phys. Lett. B* 262: 362 (1991)
11. Baglin C, et al. (NA38 Collaboration). *Nucl. Inst. Meth.* to be published
12. Abreu MC, et al. (NA50 Collaboration). *Phys. Lett. B* 410: 337 (1997)
13. Abreu MC, et al. (NA50 Collaboration). *Nucl. Phys. A* 610: 404c (1996)
14. Fleuret F. PhD thesis. Ecole Polytechnique, Palaiseau.175 pp. (1997)
15. Schuler GA, CERN-TH/94-7170
16. Alde DM, et al. (E772 Collaboration). *Phys. Rev. Lett.* 66: 133 (1991)
17. Abreu MC, et al. (NA50 Collaboration). *Nucl. Phys. A* 566: 77c (1994); Abreu MC, et al. (NA50 Collaboration). *Nucl. Phys. A* 590: 117c (1995)
18. Clark AG, et al. (E722 Collaboration). *Nucl. Phys. B* 142: 29 (1978); Antoniazzi L, et al. (E705 Collaboration). *Phys. Rev. D* 46 4826 (1992); Snyder HD, et al. (E444 Collaboration). *Phys. Rev. Lett.* 42: 944 (1979)
19. Borhani A. Ph. D. Thesis, Paris (1996)
20. Baglin C, et al. (NA38 Collaboration). *Phys. Lett. B* 251: 472 (1990)
21. Bialas A, et al. *Nucl. Phys. B* 111: 461 (1976)
22. de Jager CW, et al. *Atomic Data and Nuclear Data Tables*14: 485 (1974)
23. Freundereich K. *Intern. Journ. of Mod. Phys.A* 5: 3643 (1990)
24. Gluck M, et al. *Phys. Lett. B* 306: 391 (1993)
25. Baglin C, et al. (NA38 Collaboration). *Phys. Lett. B* 251:465 (1990)
26. Baglin C, et al. (NA38 Collaboration). *Phys. Lett. B* 262:362 (1991)
27. Badier J, et al. (NA3 Collaboration). *Z. Phys. C* 20: 101 (1983)
28. Antoniazzi L, et al. (E705 Collaboration). *Phys. Rev. Lett.* 70: 383 (1993)
29. Lourenco C. (NA38/51 Collaboration). *Nucl. Phys. A* 610: 552c (1996)
30. Binkley M, et al. *Phys. Rev. Lett.* 50: 302 (1983)
31. Buchmüller W, Tye S-HH. *Phys. Rev. D* 24: 132 (1981)
32. Braaten E, et al. *Ann. Rev. Nucl. Part. Sci.* 46: 197 (1996)
33. Fritzsch H. *Phys. Lett. B* 67: 217 (1977)
34. Barger V, et al. *Z. Phys. C* 6: 169 (1980), *Phys. Lett. B* 91: 253 (1980)
35. Gavai R, et al. *Int.J.Mod.Phys.* 10: 3043 (1995)
36. Chang C-H. *Nucl. Phys. B* 172: 425 (1980)
37. Berger EL, Jones D. *Phys. Rev. D* 23: 1521 (1981)
38. Baier R, Rückl R. *Phys. Lett. B* 102: 364 (1981), *Z. Phys. C* 19: 251 (1983)
39. Bodwin GT, et al. *Phys. Rev. D* 46: 3703 (1992)
40. Bodwin GT, et al. *Phys. Rev. D* 51: 1125 (1995)
41. Sansoni A. (CDF collaboration). *Nucl. Phys. A* 610: 373c (1996)
42. Leitch MJ, et al (E789 collaboration). *Phys. Rev. D* 52: 4251 (1995)
43. Gerschel C, et al. *J. Phys. G* 22: 1335 (1996)
44. Anderson RL, et al. *Phys. Rev. Lett.* 38: 263 (1977)
45. Sokoloff MD, et al. *Phys. Rev. Lett.* 57: 3003 (1986)

46. Gerschel C, Hüfner J. *Z. Phys. C* 56: 171 (1992)
47. Blaizot JP, Ollitrault JY. *Phys. Lett. B* 199: 499 (1987)
48. Capella A, et al. *Phys. Lett. B* 206: 354 (1988)
49. Gerschel C, Hüfner J. *Phys. Lett. B* 207: 253 (1988)
50. Bauer TH, et al. *Rev. Mod. Phys.* 50: 261 (1978)
51. Hüfner J, Kopeliovich BZ. hep-ph/9712297
52. Povh B, Hüfner J. *Phys. Rev. Lett.* 58: 1612 (1987), *Phys. Lett. B* 245: 653 (1990)
53. Low FE. *Phys. Rev. D* 12: 163 (1975); Nussinov S. *Phys. Rev. Lett.* 34: 1286 (1975)
54. Kopeliovich BZ, Zakharov BG. *Phys. Rev. D* 44: 3466 (1991)
55. Kharzeev D. CERN-TH/95-342
56. Brodsky SJ, Miller GA. *Phys. Lett. B* 412: 125 (1997)
57. Blaizot JP, Ollitrault JY. *Phys. Lett. B* 217: 386 (1989)
58. Gavin S, Vogt R. *Nucl. Phys. B* 245: 104 (1990)
59. Blaschke D, Hüfner J. *Phys. Lett. B* 281: 364 (1992)
60. Hüfner J, Simbel M. *Phys. Lett. B* 258: 465 (1991)
61. Hüfner J, Kopeliovich BZ. *Phys. Rev. Lett.* 76: 192 (1996)
62. DolejšíJ, Hüfner J. *Z. Phys. C* 54: 489 (1992)
63. Kharzeev D, Satz H. *Z. Phys. C* 60: 389 (1993)
64. Piller G, et al. *Z. Phys. C A* 343: 247 (1992), *Nucl. Phys. A* 560: 437 (1993)
65. Kharzeev D, Satz H. *Phys. Lett. B* 366: 316 (1996)
66. Frankel S, Frati W. *Z. Phys. C* 57: 225 (1993)
67. Kharzeev D, Satz H. *Phys. Lett. B* 356: 365 (1995)
68. Gavin S, Gyulassy M. *Phys. Lett. B* 214: 241 (1988)
69. Hüfner J, et al. *Phys. Lett. B* 215: 218 (1988)
70. Blaizot JP, Ollitrault JY. *Phys. Lett. B* 217: 392 (1989)
71. Bordalo P, et al. (NA10 Collaboration). *Phys. Lett. B* 193: 373 (1987)
72. Baglin C, et al. (NA38 Collaboration). *Phys. Lett. B* 268:453 (1991)
73. Kharzeev D, et al. *Z. Phys. C* 74: 307 (1997)
74. Martin AD, et al. *Phys. Lett. B* 306: 145 (1993)
75. Baldit A, et al. (NA51 Collaboration). *Phys. Lett. B* 332: 244 (1994)
76. Hashimoto T, et al. *Phys. Rev. Lett.* 57: 2123 (1986)
77. Kajantie K, et al. hep-ph/9708207
78. Laermann E. *Nucl. Phys.* B (Proc. Suppl.) 42: 120 (1995)
79. Karsch F, Petronzio R. *Phys.Lett.*193: 105 (1987); *Z. Phys. C* 37: 627 (1988)
80. Röpke G, et al. *Phys. Rev. D* 38: 3589 (1988)
81. Fingberg J. hep-lat/9707012
82. Karsch F. Satz H. *Z. Phys. C* 51: 209 (1991)
83. Satz H. Color deconfinement and J/ψ suppression in high energy nuclear collisions. Lecture at the 35th course of the International School of Subnuclear Physics, Erice/Sicily. hep-ph/9711289
84. Kharzeev D, Satz H. *Phys. Lett. B* 334: 155 (1994)
85. Kharzeev D. Nucl. Phys. *A* 610: 418c (1996)
86. Kharzeev D, et al. hep-ph/9707308
87. Blaizot J-P, Ollitrault J-Y. *Phys. Rev. Lett.* 77: 1703 (1997)
88. Peitzmann T (WA98 Collaboration). *Nucl. Phys. A* 610: 201c (1996)
89. Ftacnik J, et al. *Phys. Lett. B* 207: 194 (1988)
90. Gavin S, et al. *Phys. Lett. B* 207: 257 (1988)
91. Vogt R, et al. *Phys. Lett. B* 207: 263 (1988)
92. Vogt R, et al. *Nucl. Phys. B* 360: 67 (1991)
93. Capella A, et al. *Phys. Lett. B* 393: 431 (1997)
94. Armesto N, Capella A. *J. Phys. G* 23:1969 (1997)
95. Cassing W, Ko CM. *Phys. Lett. B* 396: 39 (1997)
96. Cassing W, Bratkovskaya EL. *Nucl. Phys. A* 623: 570 (1997)
97. Gavin S, Vogt R. *Phys. Rev. Lett.* 78: 1006 (1997)
98. Vogt R. hep-ph/9708294
99. Wong C-Y. *Phys. Rev. Lett.* 76: 196 (1996)
100. Martins K, et al. *Phys.Rev.C* 51: 2723 (1995)
101. Sorge H, et al. *Phys.Rev.Lett.* 79: 2775 (1977)

102. Hwa RC, et al. nucl.-th/9706062
103. Tai A, et al. hep-ph/9701207
104. Kharzeev D, et al. *Phys. Lett. B* 405: 14 (1997)

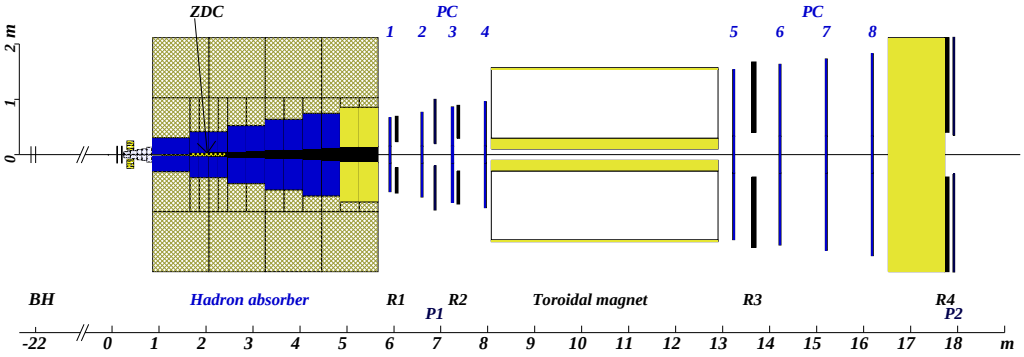

Figure 1: The set-up of the NA50 experiment.

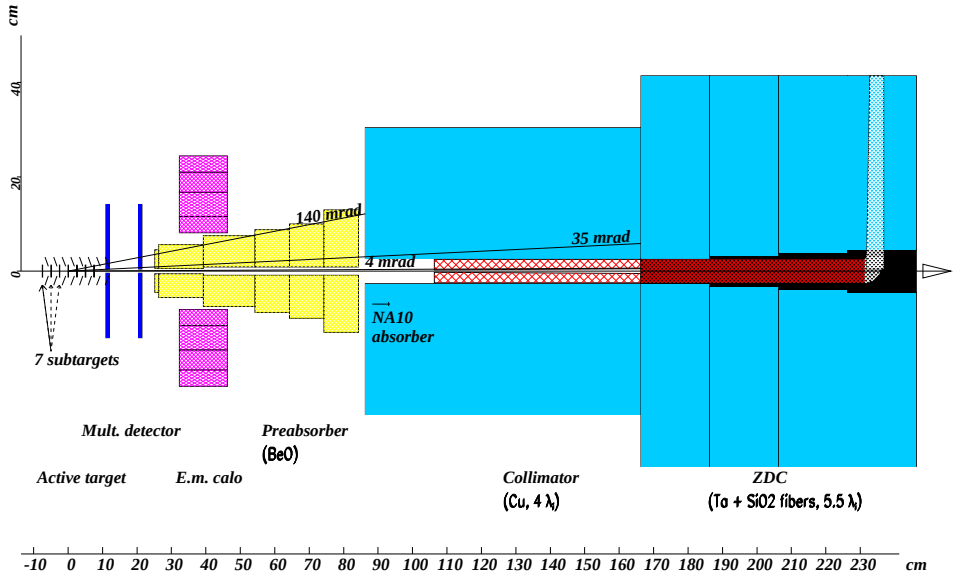

Figure 2: Lay-out of the different elements in the target area of the NA50 detector.

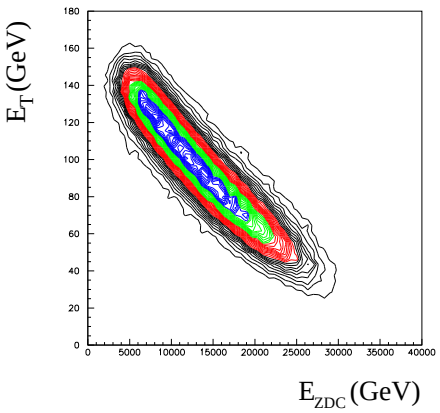

Figure 3: Correlation between the measured neutral transverse energy and the energy measured by the "zero degree" calorimeter for all events with an identified vertex.

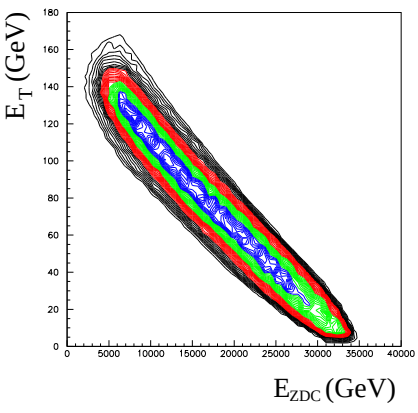

Figure 4: The same as Figure 3 for events with muon pairs in the J/ψ mass region with the method of using $E_T - E_{ZDC}$ correlation.

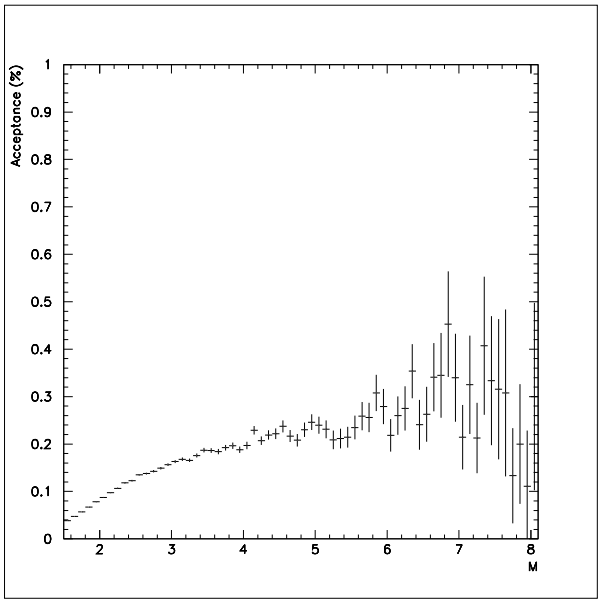

Figure 5: Acceptance of the Drell-Yan pairs as a function of the mass in *S-U* collisions.

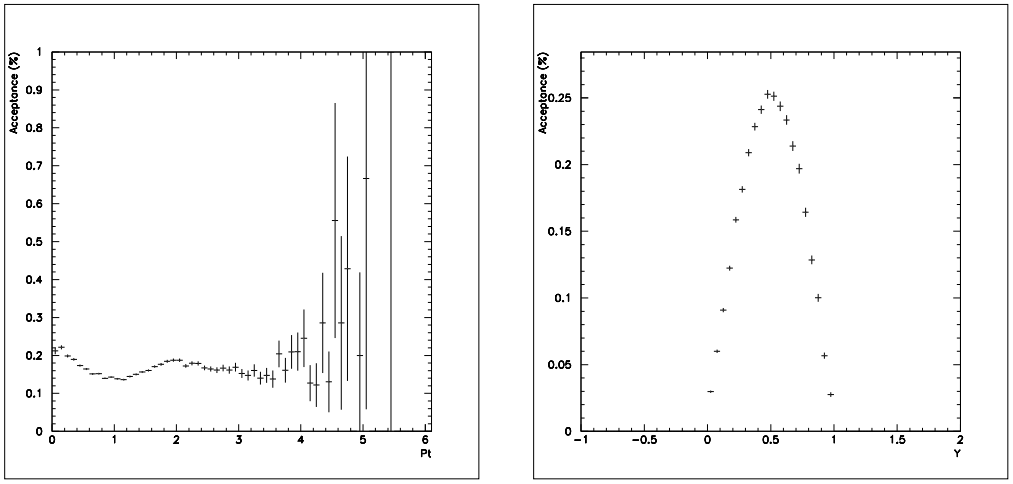

Figure 6: Transverse momentum and rapidity acceptances of J/ψ for S- U collisions

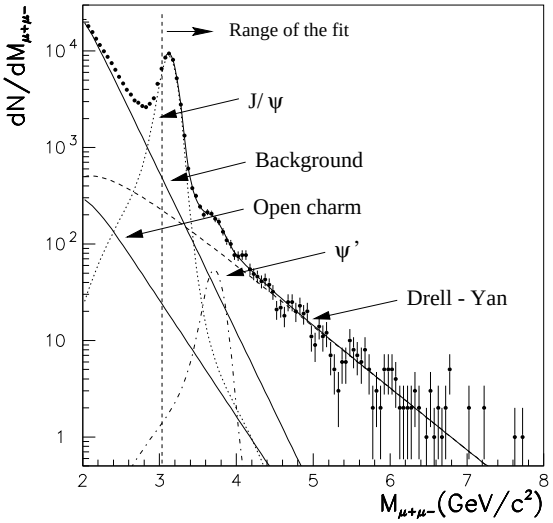

Figure 7: Mass distribution of $\mu^+\mu^-$ pairs in Pb-Pb collisions.

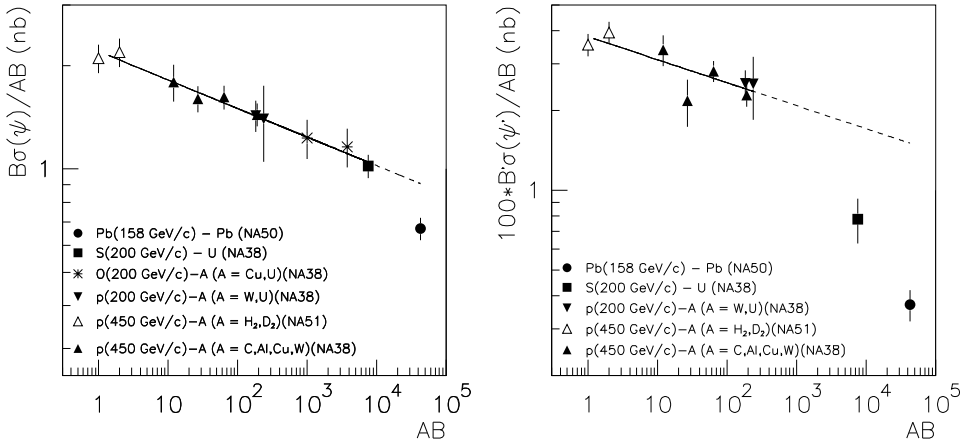

Figure 8: J/ψ and ψ' cross sections per nucleon-nucleon collisions as a function of the product of masses of target and projectile. B and B' are the branching ratio of J/ψ and ψ' decay into muons. A power law fit, $(AB)^{\alpha}$, is shown for both resonances. It includes all the points except Pb-Pb for J/ψ and only pA data for ψ' . Cross sections are all rescaled to 200 GeV as explained in the text.

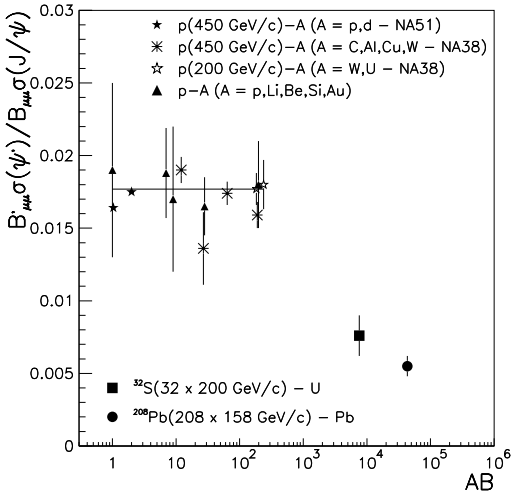

Figure 9: Ratio $B'\sigma_{\psi'}/B\sigma_{\psi}$ plotted as a function of AB. The solid line corresponds to a fit of pA data using the power law $k(AB)^{\alpha_{\psi'} - \alpha_{\psi}}$.

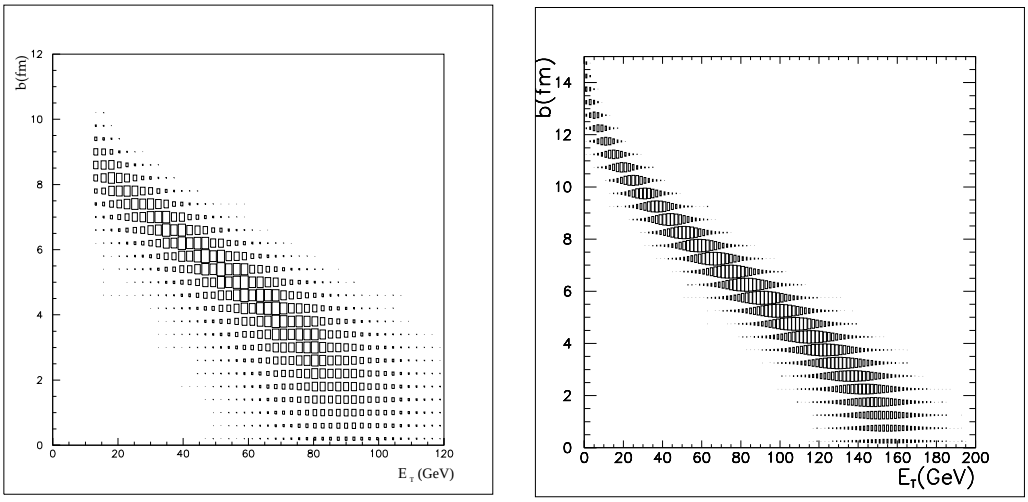

Figure 10: Correlation between the neutral transverse energy and the impact parameter for *S-U* (left) and *Pb-Pb* (right) collisions.

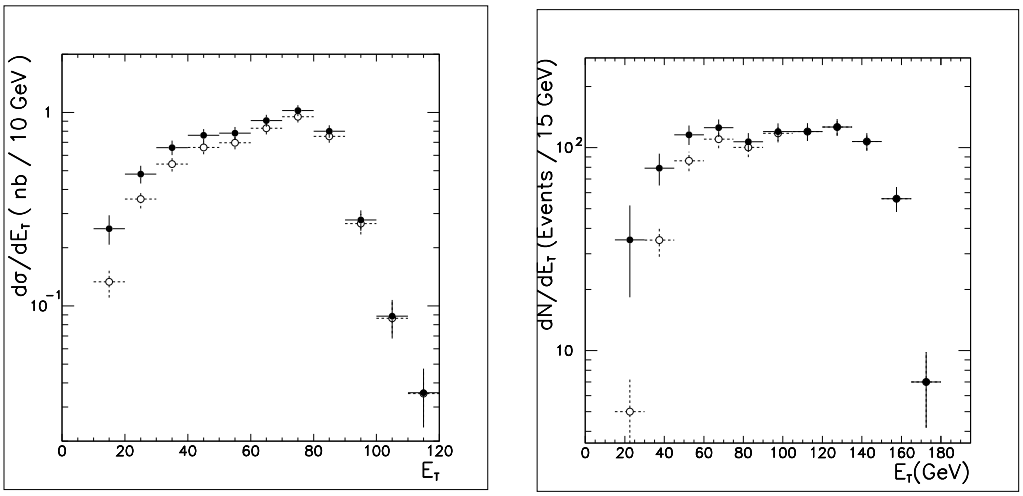

Figure 11: Transverse energy distribution for Drell-Yan pairs with $M_{\mu\mu}$ above 4 GeV/c^2 in *S-U* collisions [19] and above 4.2 GeV/c^2 in *Pb- Pb* collisions [6, 7]. The open points correspond to the raw data. The solid points are corrected for the efficiency of the "active" target.

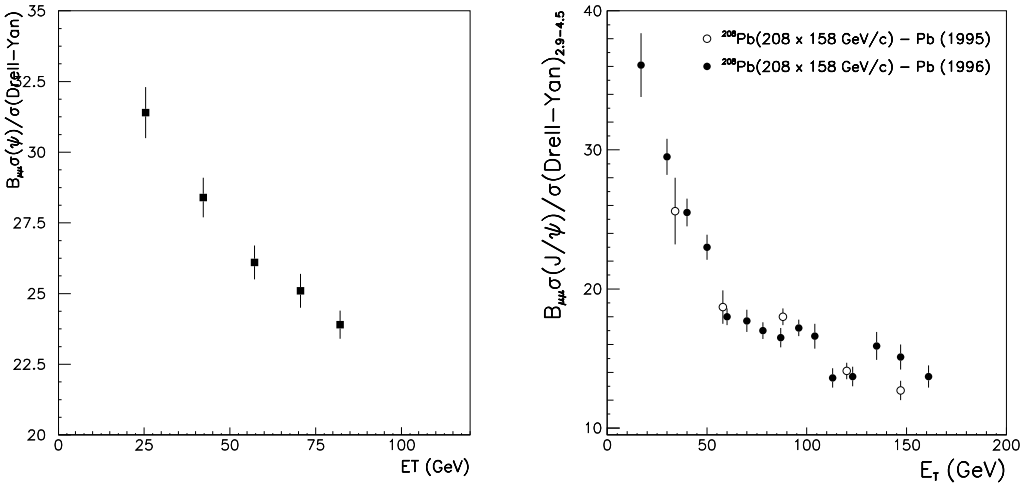

Figure 12: Ratio of J/ψ to Drell-Yan cross sections plotted as a function of neutral transverse energy for *S-U* (left) and *Pb-Pb* (right) collisions.

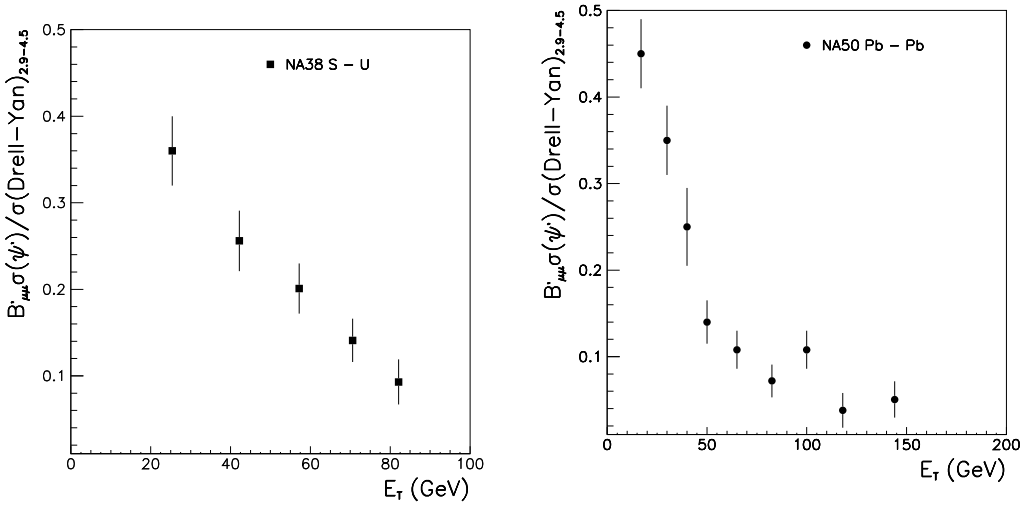

Figure 13: The same as Figure 12 for ψ' .

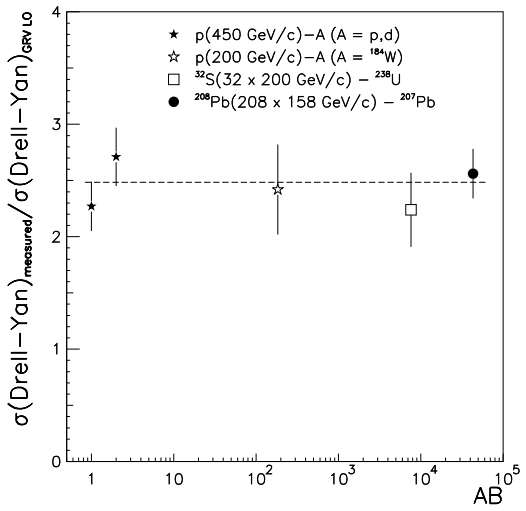

Figure 14: The Drell-Yan K-factor as a function of the product AB of the projectile and target mass numbers. The dashed line shows the average value of the data.

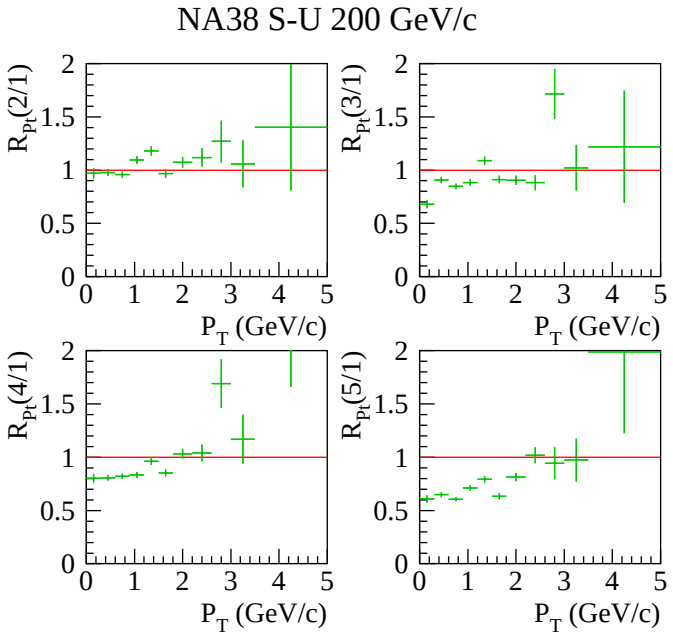

Figure 15: p_T dependence of J/ψ suppression in S-U collisions. $R_{pt(n/1)}$ gives the ratio of $d\sigma/dp_T$ for the n-th bin in E_T to the first one, normalized to the respective values of the Drell-Yan continuum in each bin.

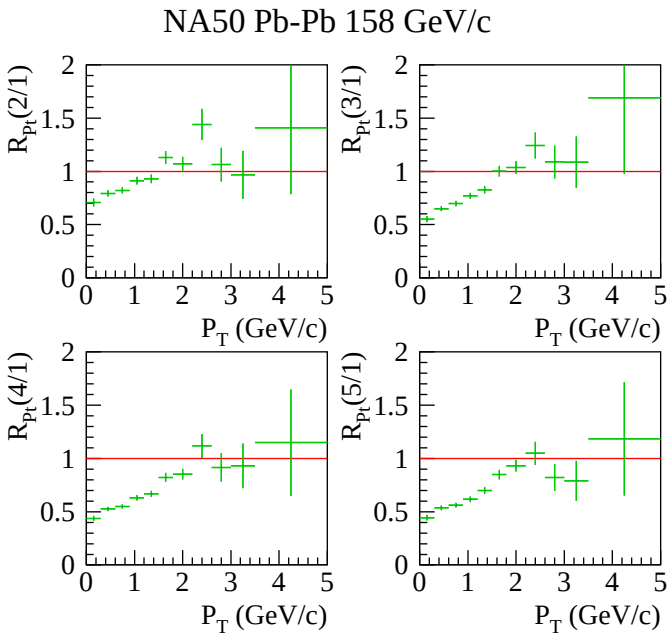

Figure 16: p_T dependence of J/ψ suppression in Pb-Pb collisions.

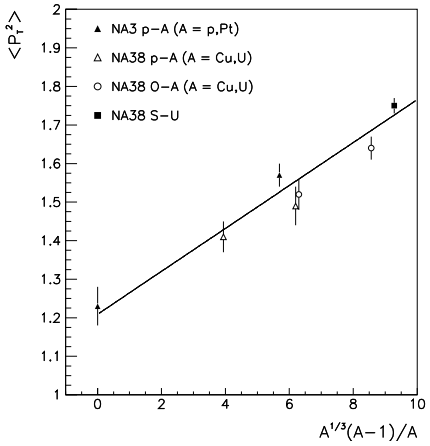

Figure 17: $< p_T^2 >$ versus $A^{1/3}$ for J/ψ . The factor $A - 1/A$ accounts for the fact that no effect is expected in pA collisions.

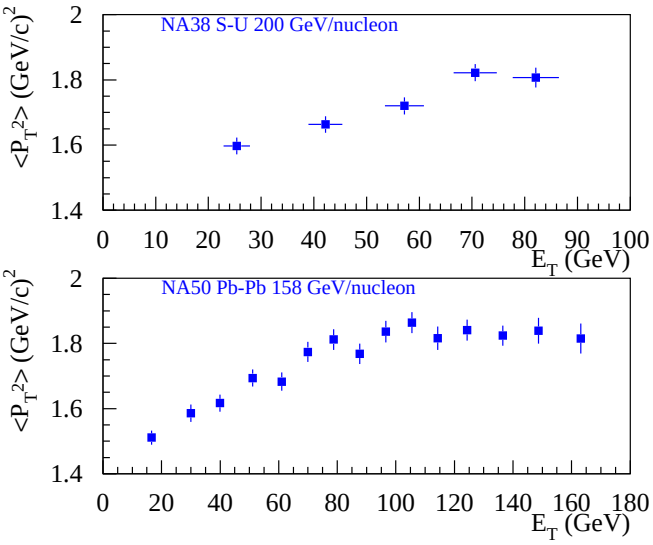

Figure 18: $< p_T^2 >$ as a function of E_T for J/ψ production in S-U and Pb-Pb collisions.

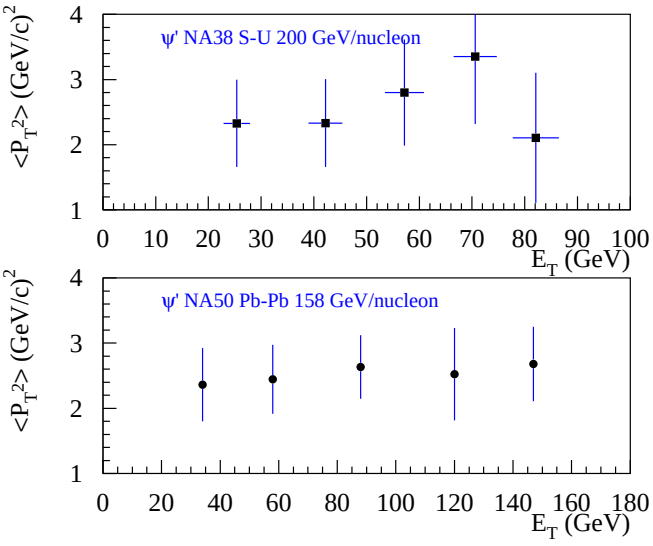

Figure 19: The same as Figure 18 for ψ' .

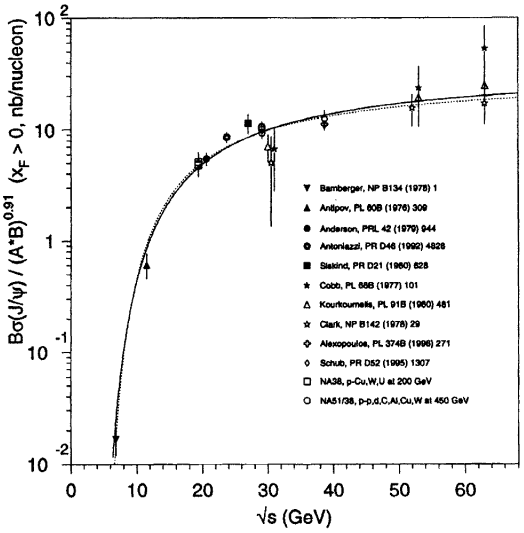

Figure 20: $\sqrt{s}$ dependence of J/ψ cross section from Reference [15].

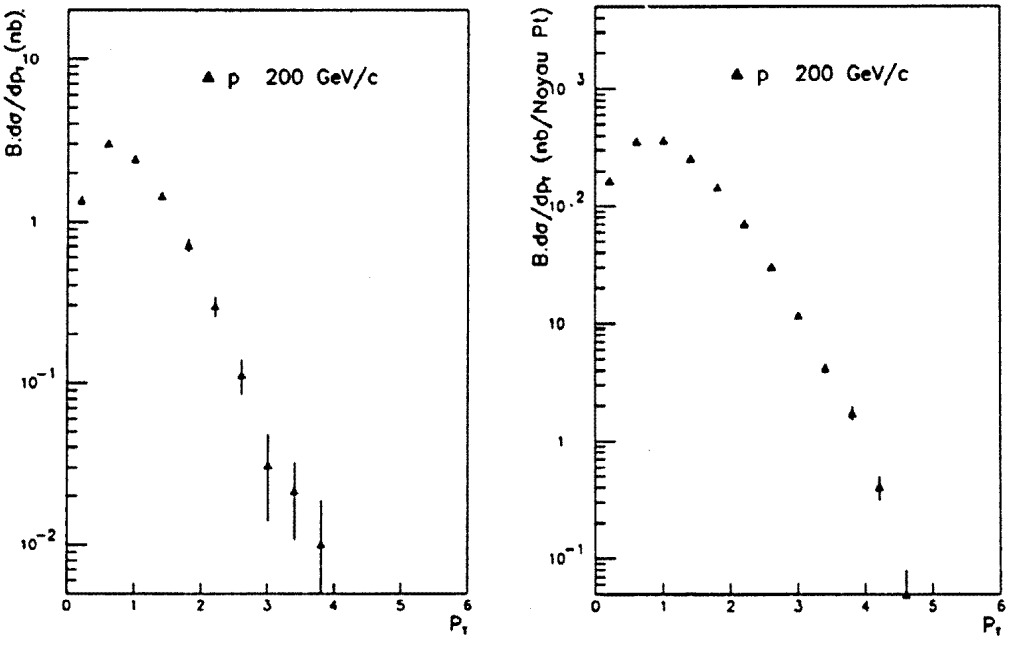

Figure 21: p_T-distribution of J/ψ for pp collisions (left) and pPt collisions (right) from Reference [27].

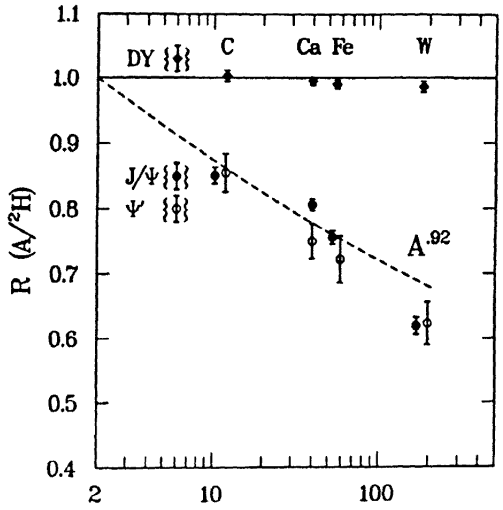

Figure 22: Nuclear mass dependence of J/ψ and ψ' production. The fits to the power law A^α are also shown. From Reference [16].

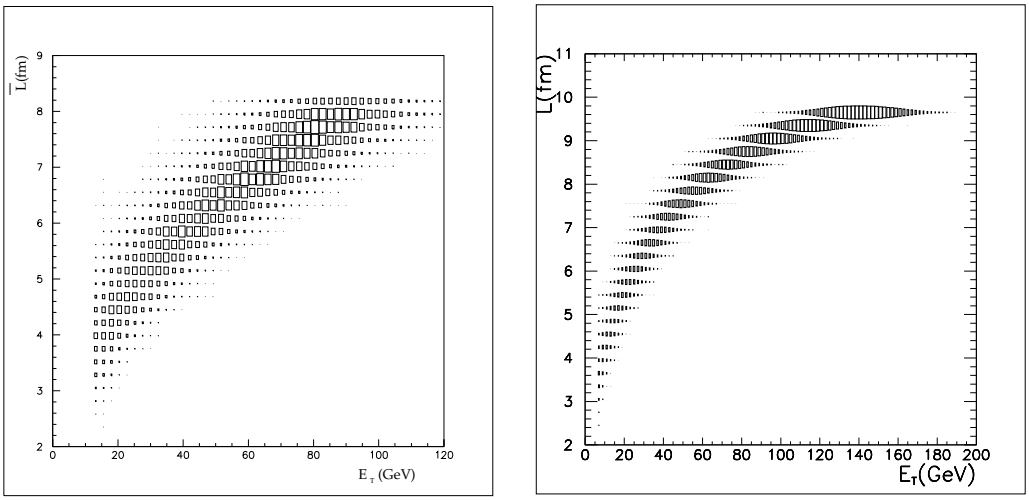

Figure 23: Correlation between the neutral transverse energy and the length of matter in the final state for S-U (left) and Pb-Pb (right) collisions.

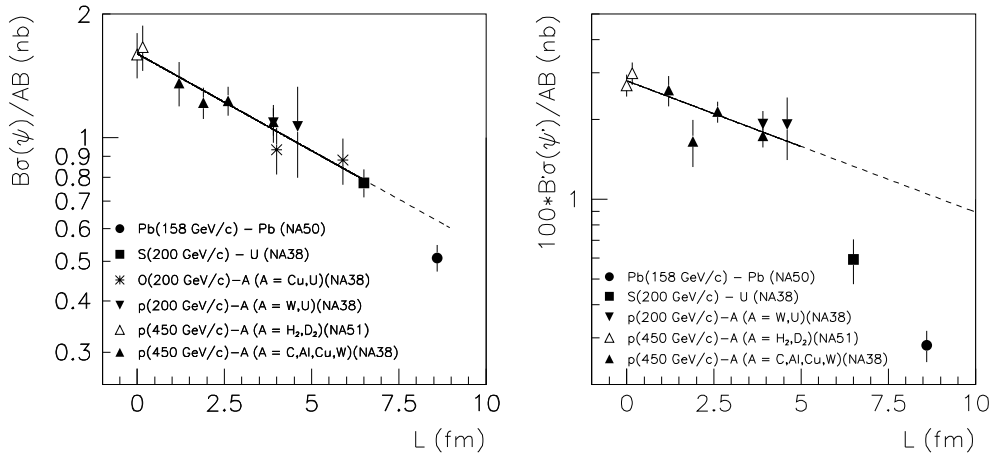

Figure 24: J/ψ and ψ' cross sections per nucleon-nucleon collisions as a function of the length L of matter in the final state. The fit to the law $exp(-\rho_0\sigma_{abs}L)$ is shown for both mesons. It includes all the points up to S-U for J/ψ and only pA data for ψ' . Cross sections are all rescaled to 158 GeV as explained in the text. The values of L are calculated with $r_0 = 1.1fm$.

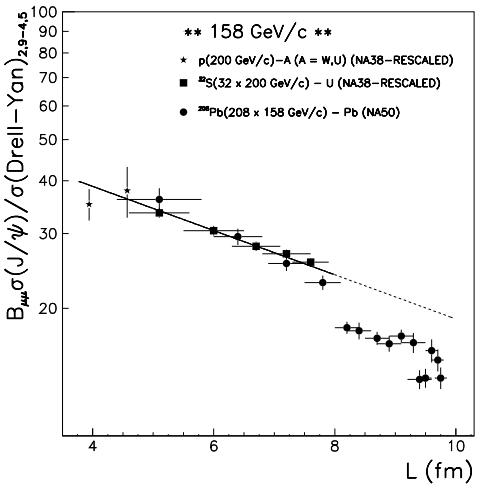

Figure 25: $B\sigma_\psi/\sigma_{DY}$ ratio plotted as a function of the length of matter in the final state. The best fit to the law $exp(-\rho_0\sigma_{abs}(\psi)L)$ is shown. It includes all the points up to SU.

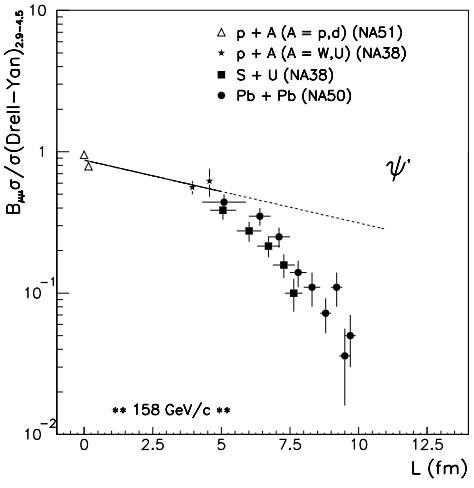

Figure 26: $B\sigma_{\psi'}/\sigma_{DY}$ ratio plotted as a function of the length of matter in the final state. The straight line is valid only for pA data.

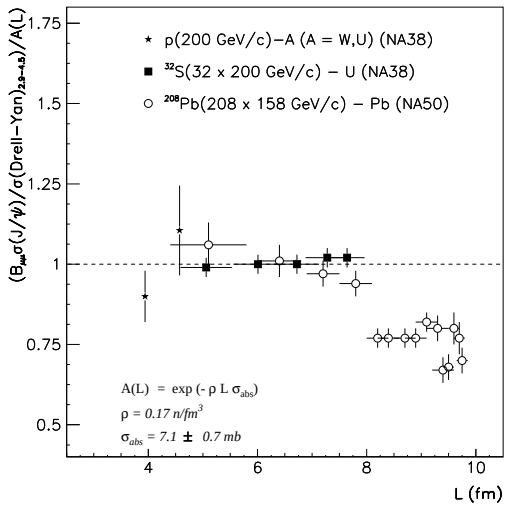

Figure 27: $B\sigma_\psi/\sigma_{DY}$ ratios at 158 GeV/c divided by the value coming from the exponential fit plotted as a function of the length L of matter in the final state.

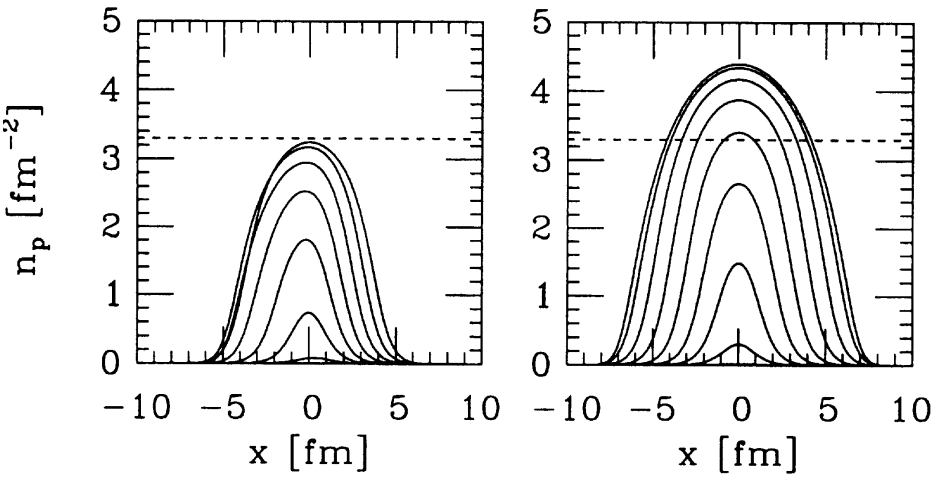

Figure 28: Density distribution of participant nucleons along the direction of the impact parameter. The solid lines correspond to density profiles plotted for equidistant impact parameters, every 2 fm. The horizontal dashed line corresponds to the critical threshold choosen just above the largest energy density achieved in S-U collisions [87].

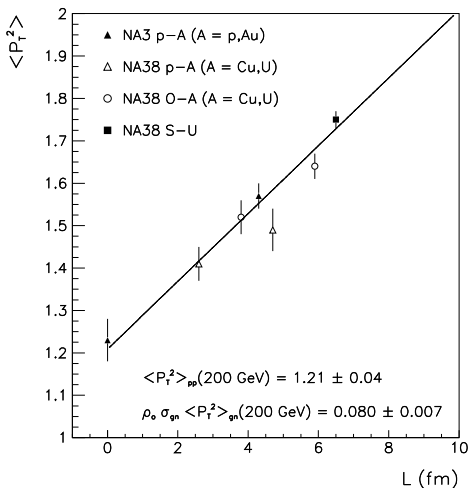

Figure 29: $< p_T^2 >$ values at 200 GeV/c without selection on the impact parameter plotted as a function of the length of matter in the final state. The solid line corresponds to the best fit to the law defined by Equation 36.

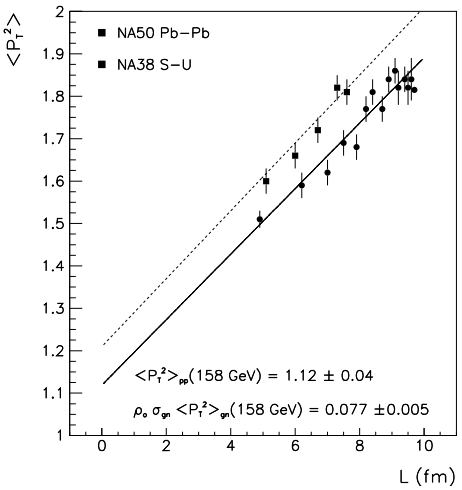

Figure 30: The same as Figure 29 for the centrality dependence of *S-U* and *Pb-Pb* collisions. The dotted line is a plot of t of Equation 36 with the parameters deduced from the fit of Figure 29. The solid line is the best fit of *Pb-Pb* data using a straight line.